Progress in Oceanography 104 (2012) 59–79

Contents lists available at SciVerse ScienceDirect

Progress in Oceanography

journal homepage: www.elsevier.com/locate/pocean

Water mass properties and dynamic conditions of the Eastern Mediterranean in June 2007

Vedrana Kovačević [a,*], Beniamino Bruno Manca [a], Laura Ursella [a], Katrin Schroeder [b], Stefano Cozzi [c], Mihai Burca [a], Elena Mauri [a], Riccardo Gerin [a], Giulio Notarstefano [a], Davide Deponte [a]

[a] Istituto Nazionale di Oceanografia e di Geofisica Sperimentale – OGS, Trieste, Italy
[b] CNR-ISMAR, La Spezia, Italy
[c] CNR-ISMAR, Trieste, Italy

ARTICLE INFO

Article history:
Received 18 May 2011
Received in revised form 23 May 2012
Accepted 26 May 2012
Available online 26 June 2012

ABSTRACT

Five locations in the Eastern Mediterranean, situated in the Ionian Sea, Cretan passage and Levantine basin, were characterized for their physical and biogeochemical properties on the basis of the data collected during an oceanographic cruise in June 2007. Basinwide, subbasin and mesoscale surface dynamic features are described in terms of absolute dynamic topography of the sea surface, sea surface temperature and chlorophyll-*a* distribution. Additional information along the ship's track was acquired via the vessel-mounted thermosalinograph and the Acoustic Doppler Current Profiler, providing data on temperature, salinity and marine current. The latter helped identify the depth penetration (<300 m) of some dynamic structures revealed by satellite imagery. The principal water mass characteristics of the Eastern Mediterranean are described in terms of thermohaline properties and inorganic nutrient concentrations. Mixing of the principal water masses at each location was estimated by means of optimum multiparameter analysis. The June 2007 thermohaline properties are compared with those from previous studies that have described the evolution of the Eastern Mediterranean Transient from the early 1990s through the early 2000s. The processes of horizontal and vertical mixing that tend to decrease temperature and salinity of the deep waters with respect to the maximum reached during or some time after the Eastern Mediterranean Transient seem still to persist in 2007.

1. Introduction

The Eastern MEDiterranean Sea (EMED) is a relatively well studied basin. It has been a focus of interest of the wide oceanographic scientific community, especially after the observed changes of its deep thermohaline circulation in the early 1990s, reported in literature as the Eastern Mediterranean Transient (EMT) by Roether et al. (1996), Klein et al. (1999), Lascaratos et al. (1999), Josey (2003) and Roether et al. (2007). The scientific interest, nonetheless, has a long history, because the Mediterranean Sea is a natural laboratory for the study of several physical, chemical and biological processes and phenomena which also act on wider temporal and spatial scales in the world ocean (POEM Group, 1992).

Recently, interest has grown in the response of this marine area to the current climatic changes, with special regard to processes that may affect carbon dioxide storage and exchange with the atmosphere, as well as their consequences on the acidification of the marine environment (CIESM, 2008). Therefore, the EMED is the subject of many observational studies, as well as a test and validation site for numerical modelling efforts dealing with various aspects of its hydrography and dynamics (e.g., Beuvier et al., 2010).

The multidisciplinary survey TMC-07-leg-III, conducted from June 13th to June 27th 2007 in the EMED (Fig. 1) on board the

Abbreviations: ACG, anticyclonic gyre; ADT, absolute dynamic topography; AdDW, Adriatic Deep Water; APEX, Autonomous Profiling Explorer; AVISO, Archiving, Validation and Interpretation of Satellite Oceanographic data; AW, Atlantic Water; CG, cyclonic gyre; CDW, Cretan Deep Water; CIW, Cretan Intermediate Water; CIESM, Commission Internationale pour l'Exploration Scientifique de la Mer Méditerranée; CNES, Centre National d'Études Spatiales; CT, conductivity–temperature; CTD, conductivity–temperature–depth; DCM, Deep Chlorophyll Maximum; *DO*, dissolved oxygen; DUACS, Data Unification and Altimeter Combination System; EMDW, Eastern Mediterranean Deep Water; EMED, Eastern MEDiterranean Sea; EMT, Eastern Mediterranean Transient; LIW, Levantine Intermediate Water; LSW, Levantine Surface Water; MedArgo, Argo Program in the Mediterranean Sea; MODIS, MOderate Resolution Imaging Spectroradiometer; NASA, National Aeronautics and Space Administration; NOAA, National Oceanic and Atmospheric Agency; OGS, Istituto Nazionale di Oceanografia e di Geofisica Sperimentale; OMP, Optimum MutiParameter Analysis; POEM, Physical Oceanography of the Eastern Mediterranean; ODPS, Ocean Data Processing System; SSALTO, Segment Sol multimissions d'ALTimétrie, d'Orbitographie et de localisation precise; SST, sea surface temperature; SBE, Sea-Bird Electronics; σ, potential density excess; *S*, salinity; SWT, Source Water Type; *T*, Temperature; θ, potential temperature; TMW, Transitional Mediterranean Water; VM-ADCP, Vessel Mounted Acoustic Doppler Current Profiler; VECTOR, VulnErabilità delle Coste e degli ecosistemi marini italiani ai cambiamenti climaTici e loro ruolO nei cicli del caRbonio mediterraneo; WMO, World Meteorological Organisation; WOCE, World Oceanic Circulation Experiment.

* Corresponding author. Address: Istituto Nazionale di Oceanografia e di Geofisica Sperimentale – OGS, Borgo Grotta Gigante 42/c, 34010 Sgonico (Ts), Italy. Tel.: +39 040 2140 292; fax: +39 040 2140 233.
E-mail address: vkovacevic@ogs.trieste.it (V. Kovačević).

0079-6611/$ - see front matter © 2012 Elsevier Ltd. All rights reserved.
http://dx.doi.org/10.1016/j.pocean.2012.05.006

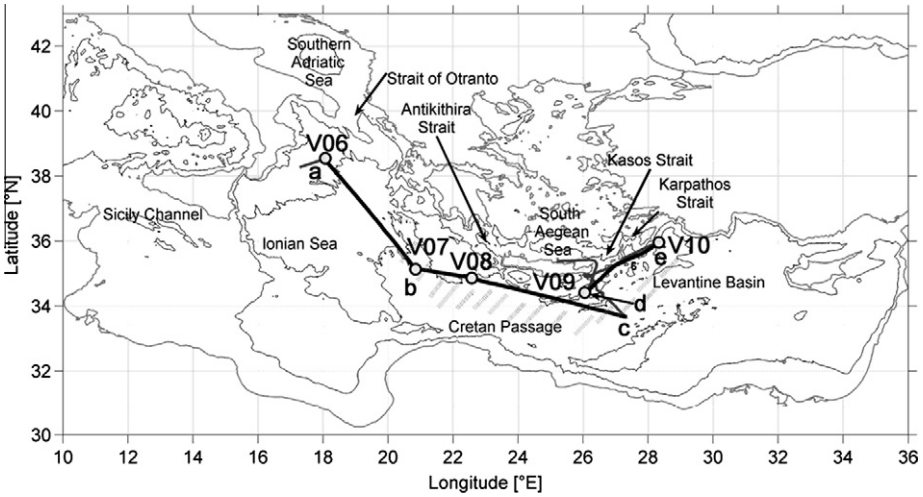

Fig. 1. Station locations during the TMC-07-leg-III cruise conducted in June 2007 in the Eastern Mediterranean. Isobaths of 1000 m and 3000 m are drawn as thin solid lines. The dashed shaded area denotes the East Mediterranean Ridge. Thick solid lines indicate the ship's track. Annotated segments refer to Fig. 9.

R/V Universitatis, was carried out as part of the TRANSMED cruise in the whole Mediterranean. The TRANSMED cruise was conducted within the framework of the Italian research project VECTOR (Vulnerability of the Italian coasts and marine ecosystems to climatic changes and their role in the Mediterranean carbon cycle – "***V**uln**E**rabilità delle **C**oste e degli ecosistemi marini italiani ai cambiamenti clima**T**ici e loro ruol**O** nei cicli del ca**R**bonio mediterraneo*"). The aim of the cruise was to perform basin-scale measurements in order to study the biogeochemical processes in the most characteristic bioprovinces of the Mediterranean (D'Ortenzio and Ribera d'Alcala, 2009), and their possible relationship with the different water mass properties and dynamics. The June survey was executed in two legs (VECTOR, 2007c, 2007d), following a similar experiment in the Western Mediterranean (VECTOR, 2007a, 2007b).

This study had the aim of a thorough description of the physical water properties, dynamic conditions and frontal systems encountered in the pelagic environment of the EMED in June 2007 (VECTOR, 2007c). One objective was to put forward, first of all, a proper frame and reference to other biogeochemical studies carried out in the EMED. The other was the state of the oceanographic conditions in 2007 as compared to those reported up to 2002.

The main water masses of the EMED (Levantine Surface Water, LSW; Atlantic Water, AW; Levantine Intermediate Water, LIW; Transitional Mediterranean Water, TMW; Cretan Deep Water, CDW; Eastern Mediterranean Deep Water of Adriatic origin, EMDW) are characterized by their thermohaline properties. The assessment of the mixing of these six water masses in the five investigated zones employed Optimum MultiParameter analysis (OMP; Tomczak and Large, 1989; Mackas et al., 1987; Karstensen and Tomczak, 1998). Moreover, the June 2007 snapshot of the EMED has been integrated into time series of long-term observations of both physical and biogeochemical properties in this basin.

In order to give as complete as possible insights into the thermohaline water properties, as well as into the typical dynamic structures of the EMED during this cruise, the *in situ* data (temperature, salinity and upper layer currents, dissolved oxygen and inorganic nutrient concentrations) are complemeted by information from satellite imagery of sea surface temperature (SST) and chlorophyll-*a* concentrations, by absolute dynamic topography (ADT) of the sea surface, and by float and drifter tracks.

These data and their treatment are reported in Section 2. Section 3 describes results and presents discussions containing: a description of the surface conditions by showing the maps of the ADT, SST and surface chlorophyll-*a* concentrations over the EMED; thermohaline properties at five locations in the EMED reported in terms of temperature–salinity diagrams and vertical profiles; surface dynamic conditions measured underway and integrated by a drifter track; principal characteristics of the circulation at intermediate depths depicted by a float track; water mass mixing and the vertical distribution of mixing fractions in the study area; and, finally, an overview of the thermohaline characteristics in June 2007 with respect to the observations available over the last two decades (from late 1980s up to 2010). Summary and conclusions are provided in Section 4.

2. Data sets and methods

2.1. CTD casts and water sampling

The acquisition system consisted of a SBE911 conductivity–temperature–depth (CTD) probe (Sea-Bird Electronics, Inc.). The probe was equipped with double pairs of conductivity and temperature (CT) sensors, a Chelsea Aquatracka fluorometer and an SBE43 dissolved oxygen sensor. It was coupled to an SBE carousel water sampler with twenty-four 10-l Niskin bottles. One of the two pairs of CT sensors was calibrated prior to and after the cruise (in February and October 2007, respectively) using the calibration facilities of OGS (Nair and Medeot, 2007).

At each station shown in Fig. 1 (V06–V10), three shallow and three deep CTD casts, on average, were performed in order to supply enough seawater volume for laboratory analyses. The permanence at each station took between 10 and 16 h, during which the spatial drift of the ship was 2–14 km.

The casts that were used for the water sampling of parameters relevant to our study [dissolved oxygen (*DO*) and nutrients] are distinguished by naming them chemical casts in Fig. 5. The nominal sampling depths in the upper layer were 2, 10, 25, 50, 75, 100, 200, 300, 400 and 500 m. In the intermediate and deep layers a 250-m step was adopted, and finally the respective near-bottom depths were sampled. The corresponding θ–S values assigned to each sample are depicted in Fig. 5c and d.

Water samples for salinity data quality control were collected at two depths at each station and analysed in the course of the cruise using a Guildeline Portasal salinometer. In addition, extra salinity samples were collected for analysis in the OGS laboratory by means of an Autosal Guildline salinometer in order to detect any

conductivity sensor drift during the campaign. A post-cruise detailed analysis of differences in temperature, conductivity and salinity between the two sensors was performed for the data limited to the layer from 500 m to the bottom. It revealed that the temperature differences between the two sensors were, in 88% of cases, within the interval [−0.001, +0.001] °C. In 85% of the cases the conductivity differences were within the interval [−0.0002, +0.0002] S/m, and in 98% of the cases the salinity differences were within the interval [−0.002, +0.002]. According to the nominal accuracy stated by the sensor producer, which was ±0.002 °C for temperature and ±0.0003 S/m for conductivity (which corresponds to ±0.005 for salinity), all data were well within the nominal accuracy.

Samples for the determination of *DO* were collected and analysed using the Winkler method (Grasshoff, 1983), using an automated potentiometric titration system (798 MPT Titrino; Metrohm). The precision of the analytical system for the analysis of replicates of reference standards ($n = 40$), expressed as a coefficient of variation, was 0.2% at the concentration level of 200 μM-O_2. These *DO* concentrations were used to adjust the values acquired by the SBE 43 sensor. This was done by fitting a second-order polynomial as a function of depth to the differences between the SBE 43 sensor and Winkler values at discrete levels. Fitted differences were then used to correct the continuous DO profile measured by the sensor.

Samples for the determination of dissolved inorganic nutrients were filtered on pre-combusted Whatman GF/C filters and placed in acid-washed HDPE vials. They were immediately frozen (−20 °C) and stored in the dark until analysis in the laboratory of CNR-ISMAR in Trieste. The determination of nitrate and nitrite ($NO_3 + NO_2$), reactive phosphorus (PO_4) and reactive silicon (SiO_2) was carried out using a Flow-Solution III autoanalyzer (OI-Analytical), following standard colorimetric methods (Koroleff and Grasshoff, 1983). The detection limit of the method was 0.01 μM for nitrate and nitrite, and 0.005 μM for reactive phosphorus and reactive silicon. The precision of the analyses varied with nutrient concentration levels, according to the values reported in the literature.

In order to depict the thermohaline properties in the study area, potential temperature (θ, °C) and potential density referenced to 0 dbar were derived from the temperature (T) and salinity (S) profiles, averaged every 1 dbar. Subsequently, σ_0 was calculated as potential density − 1000 (kg/m^3). For this purpose, TEOS-10 (http://www.TEOS-10.org) expressions implemented within the ODV (Ocean Data View; Schlitzer, 2011) were used. Moreover, potential density referenced to 2000 dbar, in terms of σ_{2000}, was introduced when describing the deep layers, especially for comparing and discussing the temporal evolution of the thermohaline properties at the considered locations.

2.2. Vessel-Mounted Acoustic Doppler Current Profiler (VM-ADCP)

A 150-kHz RDI-ADCP measured horizontal currents along the cruise track below the ship's hull. Current data were collected from the 14th to the 25th of June 2007. The instrument was set to measure currents within sixty cells, each 8 m thick, for a total depth range of about 470 m starting at 14 m depth. The acquisition time step was 2 s, but all the processing was performed over the 5-min averages. The VM-ADCP receives pitch, roll and heading data from the software PDS2000 and uses this information to re-project currents along the north and east directions. Due to a problem with this software, the heading was not properly registered and the data have been re-processed to obtain valid current data. Afterwards, the CODAS3 software (University of Hawaii) was implemented in order to edit, georeference and interpolate the current measurements over a regular spatial grid. Due to the high ship speed, the number of cells with good data was reduced to 32, and the measurement range thus reached a depth of 250–300 m. In addition, the currents from the first cell (at 14 m) were of poor quality, probably due to the turbulence produced by the ship. Mean speeds, calculated over the entire data set at each depth, were higher than 15 cm/s. As tides in the study zone are low (<5 cm/s) with respect to the magnitude of currents (Lozano and Candela, 1995; Velegrakis et al., 1999), it was not necessary to low-pass-filter the data set. Moreover, as the currents varied in both time and space, an appropriate filtering process would need a very fine time and horizontal coverage over the area (Candela et al., 1992; Ursella and Gacic, 2001), which was not the case. Therefore, currents with magnitude $\geqslant$5 cm/s were considered not to be affected by tides.

Along-track current maps were produced both vertically along defined transects and horizontally, at specific depths. Horizontal maps of currents were then superimposed on the ADT maps in order to correlate dynamic features and frontal systems.

2.3. Underway surface temperature and salinity

Continuous measurements of the surface thermohaline properties were conducted along the ship track by means of an SBE21 Thermosalinograph and SBE38 remote temperature sensor (Sea-Bird Electronics, Inc.). The nominal accuracy of the sensors was 0.001 °C for the SBE38, 0.01 °C for the SBE21 temperature and 0.001 S/m for the SBE21 conductivity, corresponding to ±0.017 for salinity. The sampling interval was 5 s. Temperature and salinity were determined for the water pumped on board from a depth of about 5 m.

2.4. MODIS imagery

The MODIS (Moderate Resolution Imaging Spectroradiometer) sensor is functioning on both the Terra and Aqua spacecraft. It has a viewing swath width of 2330 km and views the entire surface of the Earth every 1–2 days. The Aqua Ocean Level-3 binned archived chlorophyll and sea surface temperature (SST) measured using 3- and 4-μm channels were download from the NASA Goddard Space Flight Center's Ocean Data Processing System (ODPS). The spatial resolution of the products is 4.6 km. The daily chlorophyll data for the area of the Levantine basin were used to produce 8-day composites.

2.5. Drifter track

A total of 97 surface drifters were deployed in the EMED between September 2005 and March 2007, in the framework of the EGITTO/EGYPT program, to describe its surface circulation patterns (Gerin et al., 2009). The deployments occurred mainly in the Sicily Channel (at the western entrance of the channel), in the Ionian and in the Levantine.

The drifters used were the mini WOCE-SVP (model CLEARSat-15) manufactured by Clearwater Instrumentation. The surface buoy was tethered to a cylindrical drogue (with a 60-cm diameter and a 5-m height), centred at a nominal depth of 15 m. The buoy was equipped with an SST sensor and a tension sensor that allows checking for the presence of the drogue. All drifters were tracked with the Argos System.

Drifter raw data were edited for outliers and spikes with automatic and manual techniques using criteria based on maximum distance, maximum speed and maximum angle between two consecutive points, as described in Poulain et al. (2004). Edited positions were interpolated at 2-h intervals with a krigging optimal interpolation scheme (Hansen and Poulain, 1996). The interpolated positions were then low-pass filtered using a Hamming filter with cutoff period of 36 h to eliminate high-frequency current components (tidal and inertial currents), and were finally subsampled

at 6-h intervals. Velocity components were then estimated from centred finite differences of the 6-h subsampled positions.

Undrogued drifter data were corrected using linear regression models of the differences between nearly collocated and co-temporal undrogued and drogued drifter velocities as a function of wind, following Poulain et al. (2009a). The undrogued drifters generally displayed downwind slippage of about 1% of the wind speed.

In particular, the undrogued drifter a70258 that travelled across the Ionian Sea in 2007 was considered in this study because it explored the investigated area almost simultaneously with our oceanographic campaign. It was deployed in October 2006 in the western sector of the Sicily Channel (~37.4°N, 11°E) and tracked until July 2007, when it stranded on the African coast (~32°N, 25°E).

2.6. Argo profiler

An APEX (Autonomous Profiling Explorer) battery-powered profiler operated in Argo was used for description of the mid-depth circulation in the eastern portion of the EMED. The profiler was equipped with Sea-Bird CTD sensors (model 41 pumped MicroCAT with accuracies of 0.002 °C, 0.005 and 2.4 dbars for *T*, *S* and pressure, respectively). This float was employed within the MedArgo program (Argo Program in the Mediterranean Sea: Poulain et al., 2007, 2009b; Poulain and Solari, 2009; Notarstefano and Poulain, 2009), and it was set to the "Park and Profile" configuration with a parking depth of 350 m, approximately the depth of the LIW core. As maximum profiling depth, alternate values of 700 m and 2000 m were selected. At 5-day intervals the profiler ascended while measuring *T*, C and pressure, from which *S* was calculated. When at the surface (typically for 6 h), the profiler was located by, and transmited data to, the Argos system onboard polar-orbiting satellites (mostly from the National Oceanic and Atmospheric Agency, NOAA) before it descended to its parking depth and repeated the cycle. Profilers are generally designed to perform 150 cycles. In this study we made use of an APEX profiler, identified by its WMO (World Meteorological Organization) code number 6900302, which was deployed in the Levantine basin on 21 May 2005 and followed through to 31 July 2007.

2.7. Quantification of water mass fractions

The estimate of the mixing between the main water masses and the spatial distribution of mixing fractions was carried out by means of OMP analysis (Package for MATLAB, Karstensen and Tomczak, 1999). The basis and applications of the method are described by Tomczak and Large (1989), Mackas et al. (1987) and Karstensen and Tomczak (1998). Essentially, a linear system of equations (following Tomczak and Large, 1989)

$$\begin{aligned}
&\theta_1 w_\theta x_1 + \theta_2 w_\theta x_2 + \theta_3 w_\theta x_3 + \cdots + \theta_k w_\theta\, x_k = \theta_{\text{obs}} + R_\theta \\
&S_1 w_S x_1 + S_2 w_S x_2 + S_3 w_S x_3 + \cdots + S_k w_S\, x_k = S_{obs} + R_S \\
&DO_1 w_{DO} x_1 + DO_2 w_{DO} x_2 + DO_3 w_{DO} x_3 + \cdots + DO_k w_{DO}\, x_k = DO_{\text{obs}} + R_{DO} \\
&P_1 w_P x_1 + P_2 w_P x_2 + P_3 w_P x_3 + \cdots + P_k w_P \quad x_k = P_{\text{obs}} + R_P \\
&N_1 w_N x_1 + N_2 w_N x_2 + N_3 w_N x_3 + \cdots + N_k w_N \quad x_k = N_{\text{obs}} + R_N \\
&SI_1 w_{SI} x_1 + SI_2 w_{SI} x_2 + SI_3 w_{SI} x_3 + \cdots + SI_k w_{SI} \quad x_k = SI_{\text{obs}} + R_{SI} \\
&x_1 + x_2 + x_3 + \cdots + x_k = 1 + R_{Mc}
\end{aligned} \tag{1}$$

is composed of unknown fractions x_i ($i = 1,\ldots,k$) for each water mass that was considered to mix in our study zone. Every water mass was characterized by its typical values for potential temperature (θ_i), salinity (S_i) and concentrations of inorganic nutrients (phosphate P_i, nitrate + nitrite N_i and silicate SI_i) and dissolved oxygen (DO_i). The last row imposes a necessary condition for the mass conservation (*Mc*). Each parameter was suitably weighted by a coefficient *w*. Applying this linear system to each sample at discrete depths of every station, a set of fractions x_i in each sample was obtained by minimizing the residuals R_j, $j = \theta$, *S*, *DO*, *P*, *N*, *SI*.

3. Results and discussion

3.1. Surface and intermediate conditions in the EMED in June 2007

The dynamic conditions are depicted on the ADT map of the sea surface height calculated with respect to the geoid. A visual inspection of daily maps for the whole period of the cruise showed that there was no significant change in the structures. Therefore, the map in Fig. 2 for the day 20th of June 2007 was considered representative of the entire survey. We needed to take account of possible geoid uncertainties (to some extent induced by a poorer resolution of 0.5° × 0.5° [http://op.gfz-potsdam.de/grace/results/grav/g007_eigen-05c.html] with respect to the gridded ADT, 1/4°E × 1/8°N). Nevertheless, we were able to deduce some information about the EMED dynamic structure, such as dominance of high sea level in the southern Ionian and low sea level in the Levantine basin. This may be at least partially due to the generally higher density in the Levantine. In general, ADT gradients (i.e., the slope from the higher to the lower values) in the Ionian Sea are predominantly directed toward the perimeter of the basin, and in the Levantine toward the centre of the basin. At smaller spatial scales, a number of subbasin-scale structures, and among them both cyclonic and anticyclonic gyres (CG and ACG, respectively), were evident. The Pelops ACG (Robinson et al., 1991; Nittis et al., 1993; Malanotte-Rizzoli et al., 1997) was observed north of the ship's track, between stations V07 and V08. The Ierapetra ACG (Malanotte-Rizzoli et al., 1999; Özsoy et al., 1993; Theocharis et al., 1993) was crossed through at station V09. The Pelops is catalogued as a recurrent, seasonally variable, subbasin gyre to the west of Crete, while the Ierapetra one to the southeast of Crete is quasi-permanent, subject to interannual variability, as summarized in the review made by Hamad et al. (2006) on the basis of the available studies.

The dynamic features depicted by means of remotely sensed surface data were compared to the *in situ* data available in the study zone. Some of these dynamic features were well corroborated by the current measurements conducted by the VM-ADCP along the cruise track at 38 m below the surface (Fig. 2). The currents at this depth had fewer gaps with respect to shallower cells and could still be regarded as representative of the upper layer. The VM-ADCP currents, superimposed on the ADT map, in general showed a cyclonic circulation coinciding with depressions in the topography, and anticyclonic circulation corresponding to domes. In particular, currents across the Pelops and Ierapetra ACG showed their anticyclonic veering, with velocities reaching almost 50 cm/s at the gyre edge. Gerin et al. (2009) estimated from drifter tracks mean speeds larger than 30 cm/s in the area of the Ierapetra ACG.

The entire drifter track (Fig. 2) confirmed in the northern Ionian Sea a prevailing anticyclonic surface circulation that drives the path of the AW. Passing north to the Pelops ACG, the drifter showed an acceleration of its south-eastward velocity (thinning out of the track points). Station V07 was located at the edge of this gyre while station V08 seemed to be out of it. This may be the reason for different thermohaline properties encountered by the CTD profiles at these two stations. Station V09 was situated almost in the centre of the Ierapetra gyre. The temporal and spatial evolutions of the surface footprint of the Ierapetra ACG since November 2005 are well documented in Gerin et al. (2009). Another relevant feature is centred at about 39°N18°E in the northern Ionian Sea (Fig. 2). The ADT gradients established it as a CG. Station V06

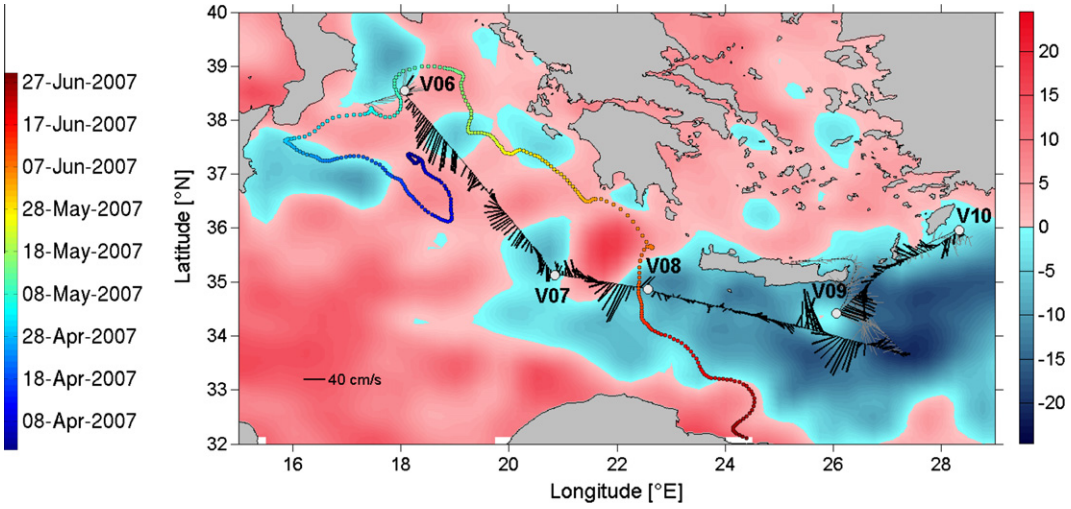

Fig. 2. Current vectors at 38 m depth derived from the VM-ADCP along the ship's track, superimposed on the ADT map. The blue–red colormap indicates ADT in cm on 20th June 2007. The colour-coded dots depict the movement of the drifter a70258 from April 2007 to the end of July 2007 (see attached legend to the left) with a step every 6 h. The timing of the ADT map is similar to the last portion of drifter track southeastward from the V08 location. The drifter passed by the V06 location in the first half of May 2007, and west of V08 in mid-June 2007. The altimeter products were produced by Ssalto/Duacs and distributed by Aviso, with support from Cnes (http://www.aviso.oceanobs.com/duacs/).

was positioned at the southern edge of this gyre, as also implied by the current data. Passing close to this structure, both drifter and VM-ADCP velocities increased (notice that drifter track in this case coincides with the beginning of May). An additional important CG in the western Ionian Sea (between 36.5 and 37.5°N and 15–18°E) was well indicated by the drifter track during April. This, and some other CG and ACG, were evident but out of the route of the cruise. Cyclonic veering of the currents in the vicinity of station V10 hinted at a cyclonic circulation along the border of the Rhodos Gyre, a further important subbasin CG (Robinson et al., 1991).

The SST distribution (Fig. 3) reflects the subbasin and mesoscale dynamic structures also seen in ADT maps: the centres of the cyclonic features are usually cooler than the surrounding areas, such as those in the central Ionian Sea at about 35.5°N, 18.5°E and at the south-western tip of Crete. Much more evident, however, was the coastal upwelling of cold waters near the southern and eastern coast of Sicily, and to the west of station V06. Moreover, the thermal front between stations V07 and V08 was clearly marked.

Complementary information on the presence of surface structures can be obtained from the chlorophyll-*a* distribution (Fig. 4). Its pattern confirms the dynamic features previously shown, although chlorophyll-*a* is also the result of the primary production processes, which often act on short temporal scales and may cause significant changes in phytoplankton biomass even within a day (Mann and Lazier, 1991). Two weekly maps were thus selected in order to illustrate its surface distribution and variability during the June campaign. Both maps indicate, in general, higher chlorophyll-*a* concentrations in the zones of prevalent cyclonic dynamics. This is a common feature that indicates a higher growth of the biomass due to the upwelling of nutrients. In contrast, zones of anticyclonic dynamics such as the southern Ionian Sea, Pelops and Ierapetra ACG, being poorer in nutrients, had lower chlorophyll-*a* concentrations. A particularly evident impoverishment in chlorophyll-*a* was found in the centre of the Ierapetra ACG between these 2 weeks.

3.2. Oceanographic properties in the study area

The θ–S diagrams from all the CTD profiles are depicted in Fig. 5a: θ ranged from 13.45 to 24 °C, while S varied between 37.95 and 39.25. The thermohaline properties allow distinction between the main water masses in the EMED. A subsurface S minimum clearly indicates the extension of AW, which spreads from the Sicily Channel into the EMED. At station V06 this salinity

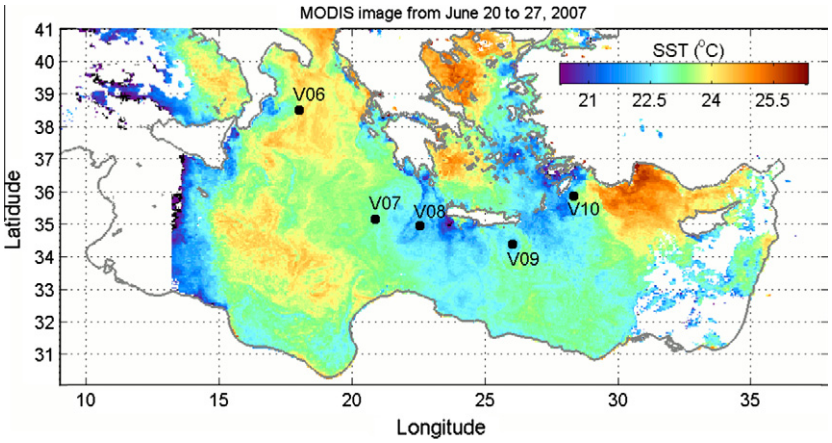

Fig. 3. SST map on 19th June 2007 and the station locations.

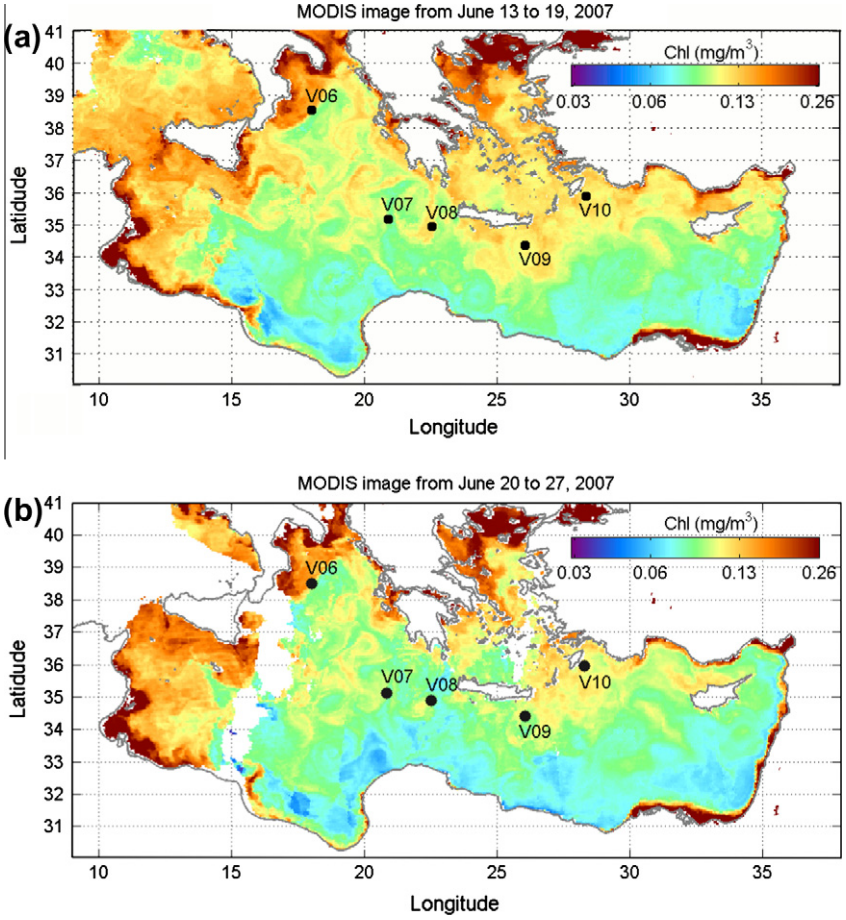

Fig. 4. Chlorophyll-*a* surface distribution during the first (a) and the second (b) week of the cruise.

minimum was most evident, and testified to the AW spreading toward the northern Ionian. Its presence was again suggested at station V08, in the Cretan Passage, where the AW branch most likely advanced due to the anticyclonic flow that characterized the northern Ionian (Fig. 2). In particular, it was turned southward by the eastern branch of the Pelops ACG, between stations V07 and V08, as corroborated by the drifter track in Fig. 2. At station V07 the presence of AW was less evident in the subsurface. Its position close to the western edge of the Pelops gyre was probably favourable to the mixing with saltier waters originating from the Aegean Sea (Theocharis et al., 1993). The surface *S* gradually increased toward the Levantine basin, where the highest values at locations V09 and V10 might be due to both the LSW and the Aegean surface water outflow.

On the basis of the θ–*S* distribution below the surface, other relevant water masses were distinguished. The presence of the LIW was identified by the *S* maximum that was observed at intermediate depths at all five stations. On a slightly denser horizon there was a TMW with *S* and θ lower than those of LIW (Theocharis et al., 1999) and more easily identified by its *DO* minimum (Fig. 6a). Finally, in the deepest layer, two distinct deep water masses were recognized, the EMDW of Adriatic origin (or simply EMDW) and the EMDW of South Aegean Sea origin (or CDW). EMDW had lower θ and *S* than CDW (Fig. 5b). The most recent EMDW has filled the deep layers of the station V06 while the CDW was present in the eastern part (V10). A detailed overview of the EMED hydrology, both pre- and post-EMT, is described in Roether et al. (2007) and references therein.

Full-depth profiles of θ, *S*, σ_0 and *DO* concentration at the five stations are illustrated in Fig. 6a. In the upper 200 m (Fig. 6b), the main feature was a seasonal thermocline located between 20 and 50 m. Below it, θ in general tended to become uniform at about 14.5 °C at all locations except at V09, where it remained notably higher due to the downwelling in the centre of the Ierapetra ACG. The *S* minima showed that the AW was found between the surface and 50 m (V06, V07, and V08). The *S* maximum was at the surface of V10 and, uniquely at this station, there was no secondary *S* maximum, which is the usual evidence of the subsurface LIW signature (Fig. 6c). Profiles of σ_0 indicated a well defined pycnocline, which separated light surface waters (26–28 kg/m^3) in the upper 30 m from the denser waters below 30 m. At V09 density was low down to 200 m (28.5 kg/m^3), in contrast to other stations (~29 kg/m^3). Profiles of *DO* are characterized by a subsurface maximum between 20 and 100 m due to biological activity (Fig. 6b). Below 150 m the oxygen content diminished, except at V09 where it remained high.

The thermohaline properties in the intermediate and deep layers (Fig. 6b–d) are characterized by an *S* maximum in the layer 150–500 m at V06, V07 and V08. At station V09 both θ and *S* remained higher than elsewhere down to 1500 m. A common feature is distinct *S* and *DO* minima at around 1000 m. A marked *DO* increase below 1000 m is due to bottom water renewal after formation and spreading of dense waters. The oxygen minimum at around 1000 m depth indicates the oldest EMDW of Adriatic origin mixed with the surrounding waters (that is, TMW), which were uplifted by the arrival of more dense waters from the Southern Aegean Sea (CDW) during the EMT in the 1990s (Roether et al., 1996, 2007; Klein et al., 1999; Lascaratos et al., 1999). The post-EMT CDW was no longer dense enough and therefore tended to remain at intermediate levels (Roether et al., 2007).

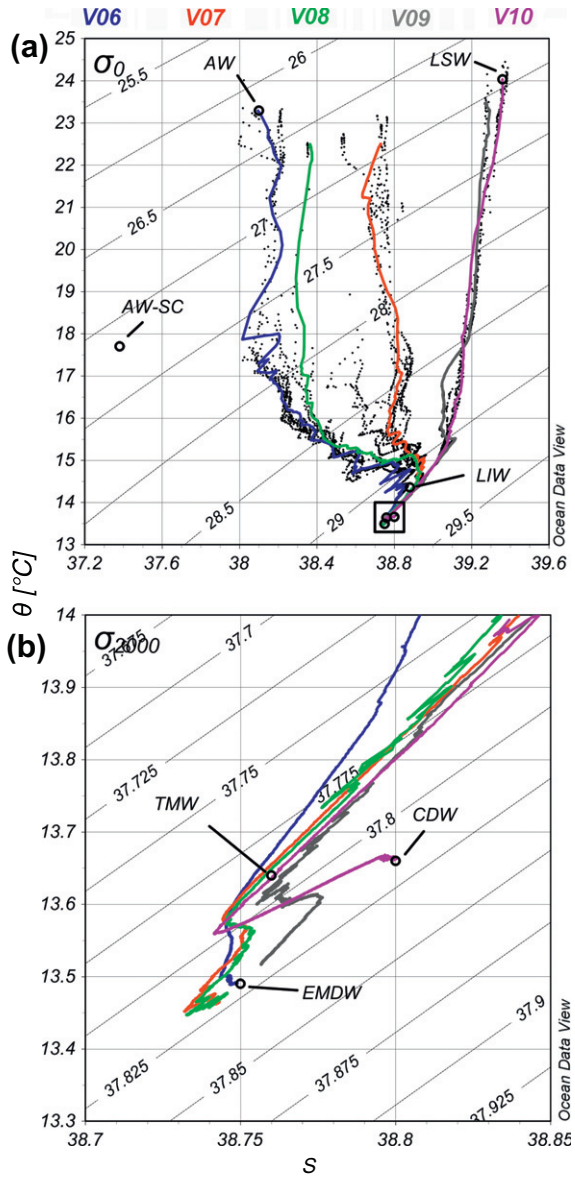

Fig. 5. θ–S diagrams from five locations in June 2007. Colour-coded solid lines indicate the casts corresponding to the sampling for oxygen and nutrients; these chemical casts were used for determining the thermohaline properties for the OMP analysis (see text). Open circles indicate the values associated with the characterisation of the water masses from Table 1. Colour code refers to the stations. (a) All available CTD profiles (black dots; there were at least five CTD casts at each location). Labelled grey dashed lines are density isolines of σ_0 (kg/m^3). The rectangle indicates the zone expanded in Fig. 5b. (b) Zoom into the deep layer of Fig. 5a using only the chemical casts. Labelled grey dashed lines are density isolines of σ_{2000}.

The comparison of the bottom S and DO content (Fig. 6d) shows that at V06, V07 and V08 more oxygenated but less saline waters were present, in contrast to what was observed at V09 and V10 (less oxygenated and saltier bottom waters). This feature was likely to be the effect of the Adriatic Deep Water (AdDW), outflowing through the Strait of Otranto, mixing with surrounding waters to form EMDW in the abyss of the Ionian Sea (Sparnocchia et al., 2011). It was distinguished by higher oxygen content and lower θ and S values than the waters still residing in the Levantine bottom layer. This recently formed EMDW had gradually spread eastward, mixing with the pre-existing bottom water, but still not reaching the two easternmost locations V09 and V10. These are located in the eastern Hellenic Trench close to the influence of the Aegean Sea dense water overflow, and they have so far been influenced by the CDW, with no renewal in recent years (Roether et al., 2007). One more observation about the EMDW detected at the stations in the Ionian Sea is of note. What is observed in the bottom layers at stations V7 and V8 (different from V06) are probably signatures of some earlier stages of the EMDW, influenced by a contribution of lower θ and S of the AdDW formed during the early post-EMT period (Klein et al., 1999).

In all the sampling sites, the vertical distribution of dissolved inorganic nutrients showed the combined effects of a strong biological consumption in the upper layer (Fig. 7a), due to the persistent summer stratification, and of the displacement of the different water masses on a subbasin scale below the thermocline (Fig. 7b). In the layer 0–50 m, the concentrations of $NO_3 + NO_2$, PO_4 and SiO_2 were low (<0.44 μM N, <0.06 μM P, <1.24 μM Si, respectively). Inorganic nutrients were also depleted from 50 m down to the Deep Chlorophyll Maximum (DCM), whose depth ranged from 70 m at station V08 to 110 m at station V07. An increase in nutrient concentrations was, instead, observed in the intermediate layer from the DCM to 1000 m of depth. Below this layer, nutrient concentrations progressively approached more homogeneous values typical of the deepest water masses (medians of 4.38 μM N, 0.18 μM P and 8.05 μM Si, respectively).

A significant exception in the vertical distribution of nutrients in the upper layer was detected at station V09, where the particularly deep nutricline (500–1000 m) was due to the downwelling of nutrient-depleted surface waters within the Ierapetra ACG. The progressive decrease in nutrient concentrations in the deepest layer observed from the east (V10) to the west (V06), matching a concomitant increase in dissolved oxygen, was a result of the different displacements of the deep water masses at larger scales.

A number of salient features of the circulation at intermediate depths in the eastern portion of our study area were described by the Argo profiler track moving at the LIW horizon at about 350 m depth (Fig. 8). During the second half of 2005 a profiler computed a cyclonic path within the Rhodos CG, apparently with low speeds. A relatively long persistence of the Ierapetra ACG (at least since the end of 2005) and its eventual spatial shift are traced back by the profiler. The track then demonstrated a prevalent westward flow through the northernmost portion of the Cretan Passage. The profiler passed V08 and V07 at the end of November 2006 and in mid-January 2007, respectivelly. It subsequently deviated southward towards the African coast, veering cyclonically between 32 and 33°N before the last fix location in the southern Ionian. One may infer that gyres play a significant role in driving and influencing properties and processes, both physical and biogeochemical ones. For instance, LIW originating in the Levantine basin, if trapped within the Ierapetra ACG, protrudes from the intermediate down to greater depths (even 1000 m) and recirculates for a certain period within it. The selected profiler indicates that the portion of LIW was trapped for about 3 months, first by the Ierapetra ACG and then by a cyclonic feature southwest of it.

3.3. Thermohaline properties and flow dynamics along the ship's track

As already shown by the SST image, temperature measured at the pump intake of the thermosalinograph 4–5 m below the surface (Fig. 9a) was also higher in the central Ionian (segment a–b) and in the Levantine basin (segment d–e) than in the Cretan Passage (segment b–c). Surface salinity (Fig. 9b) almost uniformly increased along the track from west to east. However, both temperature and salinity peaked locally, indicating salty and warm waters flowing into the Levantine basin from the Aegean Sea through the Cretan Arc Straits (segment d–e, at 26.4°E and 27.4°E). In contrast, a drop in T and S due to the local dynamic features was observed along the segment d–e (at 26.5°E and 27.5°E).

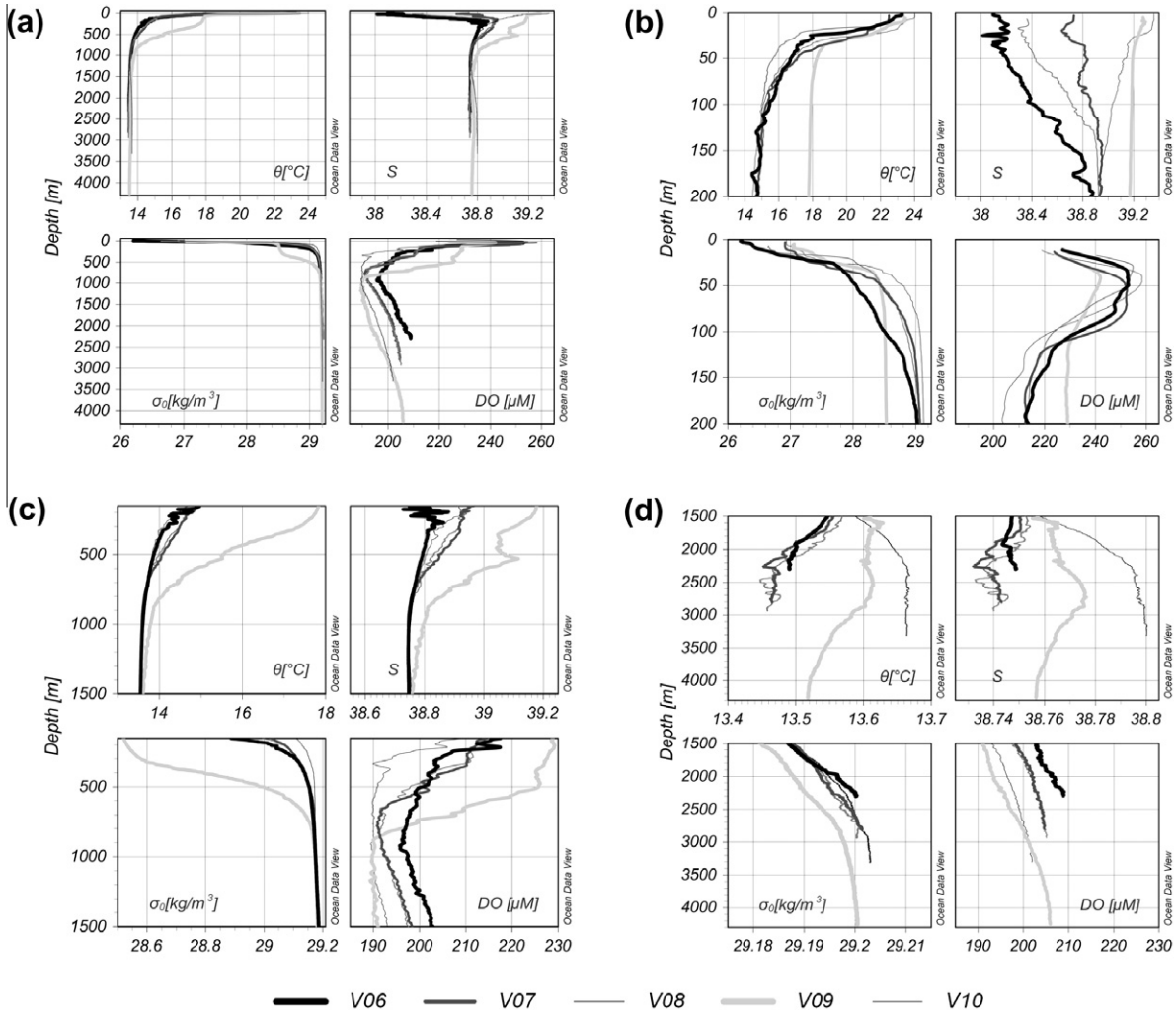

Fig. 6. Vertical profiles of θ, S, σ_0 and DO: (a) the entire profile; (b) surface layer 0–200 m; (c) the intermediate layer 150–1500 m; (d) the deep layer 1500 m-bottom. Black–grey colour code refers to the stations. Note that the scales along the x-axis are different.

The vertical distribution of horizontal currents measured by the VM-ADCP along the main segments of the ship track is depicted in Fig. 9c. Currents had the strongest magnitudes in the two ACGs, Pelops (between V07 and V08) and Ierapetra (V09) along the segment b–c, as well as in the central Ionian (between V06 and V07) along the segment a–b. Current speed reached 70 cm/s in the south-westward direction in the Pelops and 90 cm/s in the northward direction in the Ierapetra. The cyclone in the central Ionian had maximum southwestward velocities of about 55 cm/s (~18.7°E). The flow field was rather uniform with depth, at least in the first 200 m.

The segment d–e (Fig. 9c), which denotes the westward pathway from the station V10 toward V09 (thick line in Fig. 1), crossed the Karpathos Strait (~27.5°E) and the eastern part of the Kasos strait (26.8°E). A few days earlier both areas were crossed on the eastward way toward V10 (thin line in Fig. 1). We inferred that the flow across the Karpathos Strait was highly variable in both space and time. The currents that were measured in the Karpathos Strait along the d–e segment indicated a net inflow into the southern Aegean (~27.5°E, Fig. 9c), while a weak outflow (not shown) was measured during the eastward path (thin line in Fig. 1). The observed variability (within a 4-day period) is similar to the results of Kontoyiannis et al. (1999), who studied the flow through the Cretan Arc Straits on the basis of VM-ADCP and moored current-meter measurements conducted during the period 1994–1995. They found that the circulation within the first 200 m is controlled by local features and that it can be rather variable in the easternmost Cretan Arc Straits (corresponding to the segment d–e in Figs. 1 and 9c). They showed that the time-averaged upper flow at the westernmost end of the Karpathos Strait corresponded to the inflow of the LSW into the south Aegean Sea, due to the influence of the Asia Minor Current. The Asia Minor Current was defined and studied in detail by Özsoy et al. (1993). However, during June 1994 an alternating inflow and outflow on a time scale of few days was observed within the upper layer, similar to what we saw in our measurements.

In addition, Kontoyiannis et al. (1999) demonstrated that a complex interaction between the East Cretan Cyclone (within the south Aegean Sea), the Ierapetra ACG and the westward extension of the Rhodos Gyre resulted in a variable flow regime in the Kasos Strait. On a seasonal time scale, they noticed a net inflow into the south Aegean Sea in autumn and early winter and an outflow in early spring and summer. In particular, in June 1994 an alternating inflow and outflow on a time scale of a few days was observed in the surface layer in the eastern Kasos Strait (similar to that of the eastern Karpathos Strait). Such inflow-outflow variability, also evident in our data for the Karpathos Strait, was not observed while crossing the eastern part of the Kasos Strait (Figs. 9c and 1); we measured an inflow both during the westward d–e segment (~26.8°E, Fig. 9c) and earlier, while running eastward (not shown; thin line in Fig. 1).

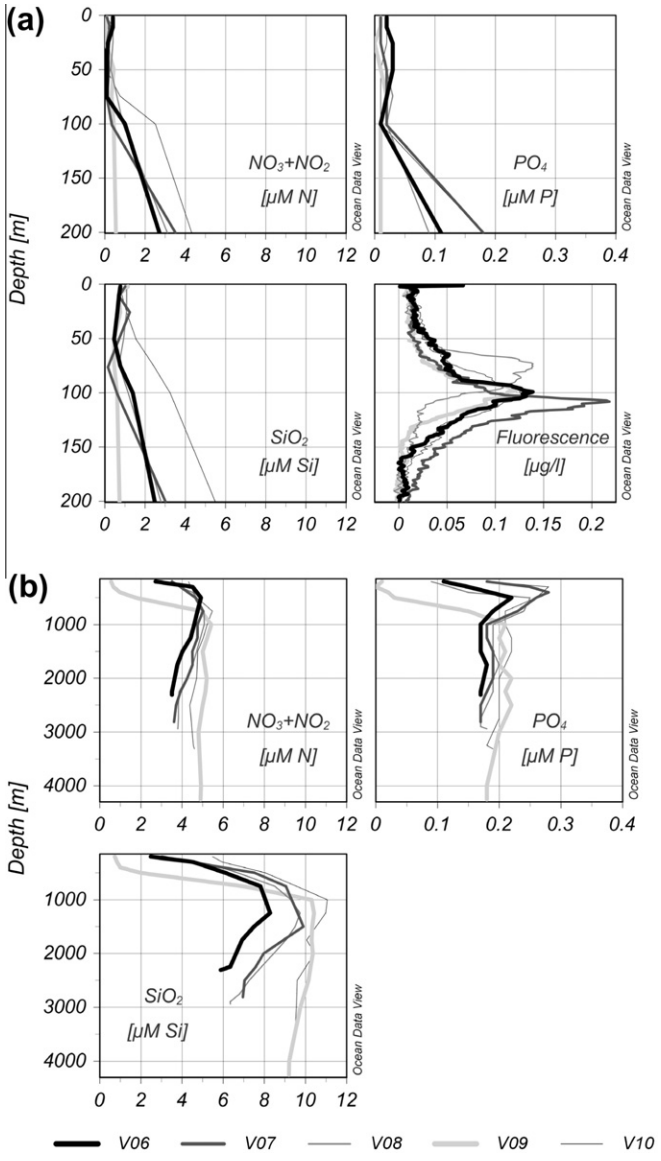

Fig. 7. Vertical profiles of nutrient concentrations at sampling depths: nitrate + nitrite ($NO_3^- + NO_2^-$, µM N), reactive phosphorus (PO_4^{3-}, µM P) and reactive silicon (SiO_2, µM Si): (a) surface layer 0–200 m including fluorescence (µg/l) and (b) intermediate–deep layer from 150 m to the bottom. Black–grey colour code refers to the stations.

3.4. Mixing fractions of the major water masses

The sea water properties in the study area were attributed to the variable mixture of the six main water masses contributing to the water body of the EMED, namely AW, LSW, LIW, TMW, EMDW and CDW. These water masses form the two main thermohaline cells of the EMED: (i) the open conveyor belt in the upper layers originating from the spreading of AW, LSW and LIW from their source regions prevalently in the east–west direction; and (ii) the deep closed thermohaline cell, driven by dense water formation, involving EMDW of Adriatic origin and CDW, as they spread predominantly southward from their formation regions (POEM Group, 1992; Roether et al., 1996). In between, the TMW (Theocharis et al., 1999) was not ventilated but was slowly transformed by vertical mixing. Each sample measured along the vertical at the five stations is considered to be a mixture containing different fractions of some or all of the six water masses.

The first step of the OMP analysis is definition of the characteristics of Source Water Types (SWTs). SWTs are defined ideally by a set of unmixed water properties in the proper region of origin (Tomczak and Large, 1989; Karstensen and Tomczak, 1999). This means that the SWT properties (such as temperature, salinity, and oxygen) of each water mass should be determined in its source region (Sicily Channel for the AW, Strait of Otranto for the EMDW, Cretan Arc Straits for the CDW, Rhodos gyre, or in general the Levantine basin for the LSW and LIW, for instance). In addition the SWTs should also be defined reasonably far back in time with respect to the period that has to be investigated, in order to take into account the mixing with the surrounding waters along their dispersing pathways from the respective source regions. The most appropriate way should be to have adequate observational data for a number of preceding years, in order to assess the time scales of the renewal and of deviations from the steady state for each particular water mass (i.e., as in Schroeder et al. (2008)). However, this was not possible in our study. Another approach may be based on the typical climatological values of the SWTs, assuming that there is no significant temporal variability of these properties; this is also a critical hypothesis. The data set of June 2007 is a snapshot of the state of the EMED as well as of the state of its main water masses. Some of these water masses are relatively stable in time but some of them have high seasonal and/or long-term variability.

The assessment of the evolution of each main water mass in the EMED that contributed to the June 2007 distribution is a complex topic requiring due attention and dedicated study involving the collection of all available historical data, which is beyond the scope of the present study. As such, we simplified the approach, assessing the properties assigned to the water masses using the June 2007 data set itself, with the intention of describing essentially a relative picture of the prevailing state of water mass distribution. This choice necessitates a caution regarding the meaning of the characteristics assigned to the actual water masses. They would be, to a certain extent, a result of processes such as mixing far from their respective source regions and the temporal variability of the source values themselves, rather than the SWT characteristics intended as point-wise end-member values. Thus, instead of using characteristics of the SWTs (regarded as point-wise values), we mostly use the mean properties that characterize the water masses. The approach of defining the water mass properties based on the June 2007 data is described in the following section.

3.5. Water mass properties and weights

The data relevant to this section are values such as θ, S and Do concentration, complemented by dissolved inorganic nutrient values (phosphate, nitrate + nitrite, silicate), referring to the discrete sampling depths of the chemical casts (see Section 2.1 and Fig. 5). The mass conservation criterion is included, to resolve the linear system of equations (Eq. (1)) for mixing between a finite number of water types (Tomczak and Large, 1989; Manca et al., 2006). Even though nutrients and oxygen are not completely conservative parameters (unlike temperature and salinity, which change only by mixing processes), they were included in the analysis as auxiliary water mass tracers. This approach is known as classical OMP analysis (Tomczak and Large, 1989). Consideration of the biogeochemical changes related to time, as well as introduction of the time-dependent tracers, in order to also determine the age of the mixed water masses, are described in Karstensen and Tomczak (1998). Moreover, van Aken (2000) utilized expressions to construct quasi-conservative biogeochemical parameters by a suitable linear combination of oxygen and dissolved nutrient concentrations, obtaining so-called preformed nutrients. Such research would require a profound investigation of the biogeochemical relations in our study region, but again this was beyond our scope.

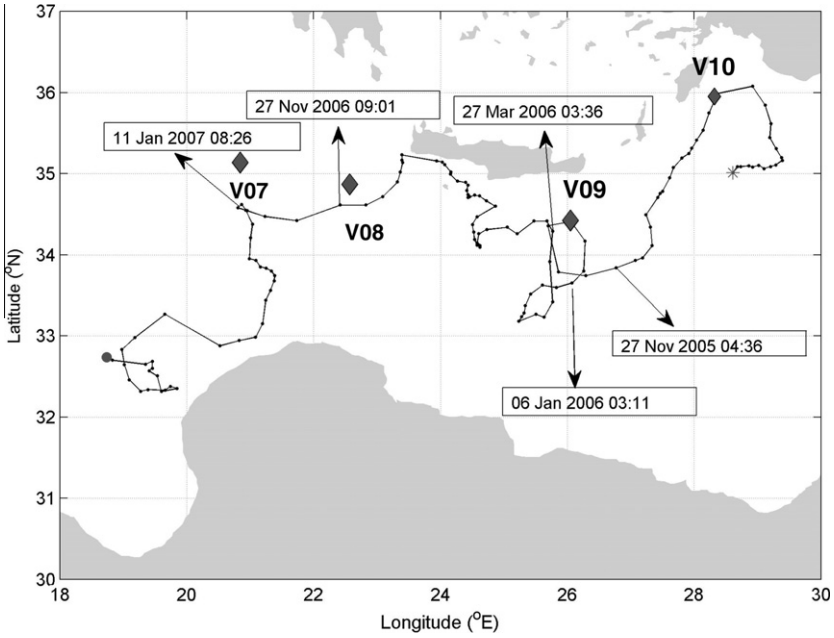

Fig. 8. Intermediate-layer circulation at 350 m derived from the Argo profiler WMO 6900302. Star and circle indicate deployment and last fixed location, 21 May 2005 and 31 July 2007, respectively. Diamonds indicate the station locations. Some intermediate passing times are indicated along the profile track.

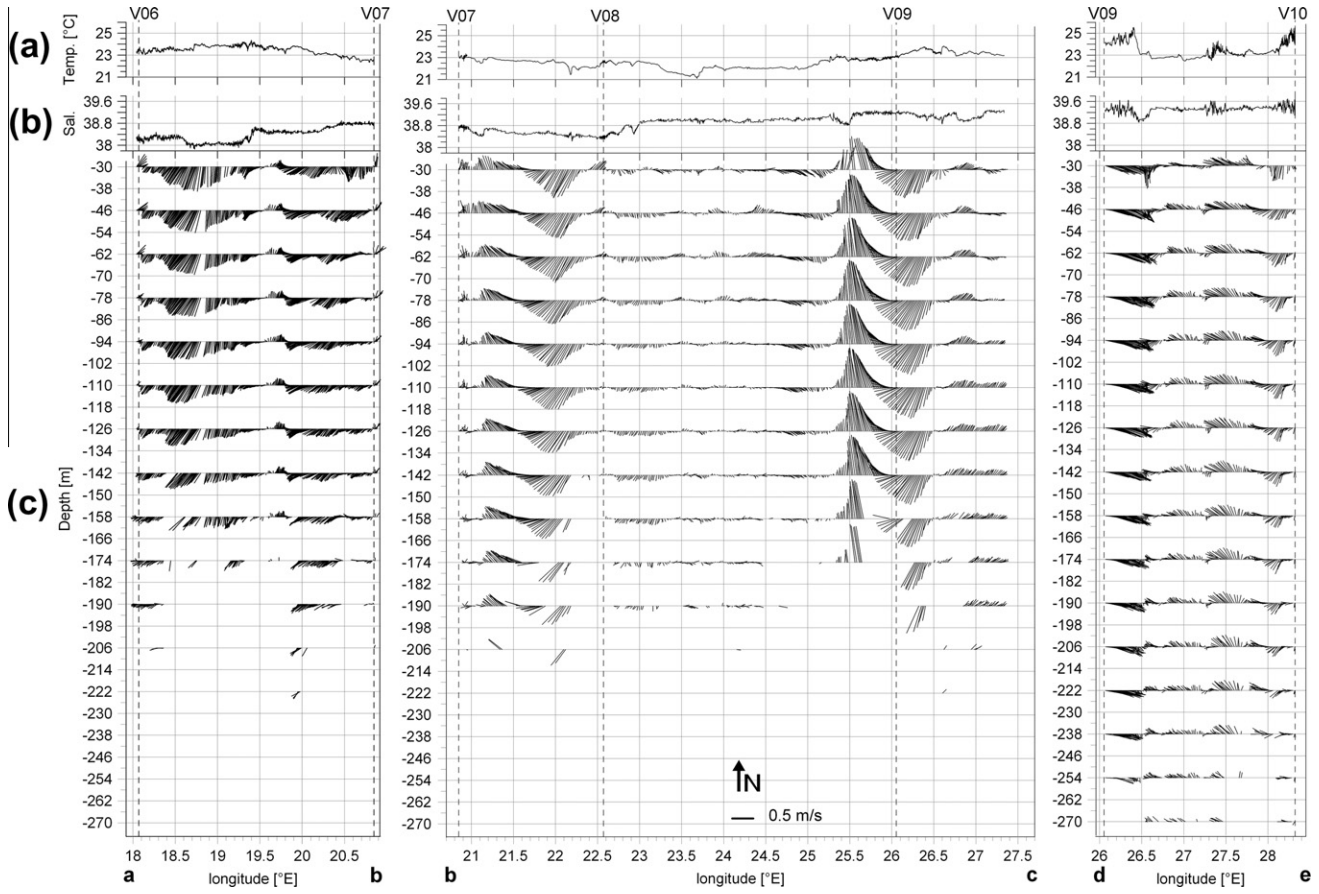

Fig. 9. (a) Surface temperature and (b) salinity from the thermosalinograph. (c) Vertical distribution of VM-ADCP currents, subsampled every 16 m. Data are reported for the three along cruise section segments a–b (left), b–c (centre) and d–e (right) indicated in Fig. 1.

In order to best characterize the six water masses, two approaches were adopted. One regards the water masses with their snapshot properties within the study area, bearing in mind that these properties are the result of previous mixing. It is based exclusively on the discrete sample values of six parameters at five stations. The data set was divided into horizontal layers of a certain thickness, and grouped according to the zones of the EMED that would be best representative of each water mass. This was accomplished for the EMDW, CDW, TMW and LIW. The surface waters are much more variable in time, so for the LSW the second approach

based on the end-members was adopted, i.e., the values associated with the sample with the highest salinity in the surface layer are taken as representative. A distinction was made for the AW. This water mass is particularly sensitive both to seasonal variations and to the mixing with the ambient waters along its pathway, which for the history of our study was a northeastward pathway from the Sicily Channel (SC). Therefore its contribution was taken to consist of two parts: one from the Sicily Channel and the other from V06, termed AW–SC and AW, respectively. Analysing some historical data it was decided to retain the average of the June 2004 and June 2006 data sets that satisfied the criterion $S < 37.5$ in the upper 50 m of the Sicily Channel as representative of the AW–SC (datasets from CNR-ISMAR cruises TRENDS and MEDOCC06, described in Vetrano et al. (2010) and Schroeder et al. (2008), respectively). The second contribution was defined as an end-member with salinity minimum and other corresponding parameters at station V06.

The values of each parameter, as representative of the water mass properties, are reported in Table 1. There is also a brief summary of how these numbers were obtained. Each of the θ–S pair associated with the water mass definitions is then depicted on the θ–S diagrams of the CTD casts in Fig. 5, as well as on the θ–S diagrams of the discrete water samples in Fig. 10a. Morover, the discrete values characterizing the chemical properties of each sample taken into consideration for the OMP analysis, as well as typical water mass properties, are plotted in Fig. 10b–e.

Another important issue for the successful outcome of the OMP is the determination of the weights for Eq. (1). Following the procedure described in Tomczak and Large (1989), the weight for each parameter was calculated in the following way: first, the mean properties of each water mass and appropriate variances were determined within a specific layer at specific stations. This has already been done for all but the surface water masses (see Table 1). Therefore the statistics were completed considering the upper 100 m, at V06 for the AW and at V09 and V10 for the LSW. The largest variance of the same parameter among the six different water masses is represented by var_2. The variance associated with the overall mean (the average of the six different mean values associated with the six different water masses) is represented by var_1. The ratio between var_1 and var_2 is the weight for each of the properties in Eq. (1). Ultimate adjustments have been made to set the temperature and mass conservation weights equal to that of salinity, and to re-dimension the weights of nitrate + nitrite and silicate to the value of the *DO*. Lower weights of the chemical properties with respect to the conservative parameters temperature and salinity reflect their lower significance as well as a higher uncertainty assigned to their low concentrations. The definitive weight values were then normalized (to sum to 100) and final estimates are reported in Table 1.

3.6. Vertical distribution of water mass fractions

The vertical distribution of the mass conservation residuals at five stations is shown in Fig. 11. They quantify the goodness of the mass fraction estimates through the adopted SWT model. Most of the values are within 8%. There are few outliers reaching 10% which are distributed among V07, V08, V09 and V10 at depths between 1000 and 1500 m. They most likely indicate the inadequately defined or not well resolved water mass properties for this layer. In another similar study, for instance, Manca et al. (2006) reported the mass conservation residuals within 8%. They applied the OMP to quantify the principal water masses' mixing in the Ionian and in the southern Adriatic Seas in 2002. The mixing of the water masses within the southern Adriatic Sea for each of the four cruises between November 2006 and October 2008 (Cardin et al., 2011) was accomplished with residuals not larger than 15%. Taking into account the limits associated with the initial hypothesis on the mixing processes, on the available data set, and possible uncertainties of the non-conservative variables, it follows that the mixing fractions of the six main water masses in our study are a reasonably acceptable result for the EMED region.

The vertical distribution of the mixing fractions for the six water masses is plotted in Fig. 12 by the shaded contouring, though one needs to bear in mind that in the areas between adjacent stations the interpolation might not be realistic.

The OMP analysis was first done for the upper 800 m, involving AW (as a sum of the two contributions, in the Sicily Channel and at V06), LSW, LIW and TMW. The relative fractions of AW and LSW in Fig. 12 refer to this run. The second OMP run was limited to depths greater than 800 m, involving AW, LSW, LIW, TMW, EMDW and CDW. The relative contributions of LIW and TMW in Fig. 12 were obtained by merging the fractions from the upper and deep run, while EMDW and CDW fractions in Fig. 12 refer to the deep run.

AW dominated the upper 100 m at V06 with fractions between 50% and 70%, and was gradually diluted further eastward (Fig. 12). At V08 there was again the signature of its presence at the surface (>40%). This is consistent with the vertical distribution of the thermohaline properties at V08 ascribed to a branch of AW circulating along the periphery of the north-eastern Ionian Sea (Fig. 2).

LSW occupied larger portions of the upper layers at V09 and V10 (50–70%) and to a lesser extent (40%) at V07 (Fig. 12). It is evident how the fractions of AW and LSW alternate at V08 and V07. Moreover, due to the downwelling in the Ierapetra ACG the signature of LSW at V09 was observed down to 600 m.

The LIW core was confined mainly in the layer between 200 and 600 m all over the region (Fig. 12). Only at V09 were there discontinuities in both its percentual content and core depth, which protruded down to 750 m (due to downwelling within the Ierapetra ACG). Such a feature is a possible signature of the LIW spreading

Table 1
Properties and weights of the principal water masses used for the OMP analysis. All properties are depicted in Fig. 10, while potential temperature and salinity are also given in Fig. 5. AW: Atlantic Water; AW–SC: Atlantic Water–Sicily Channel, LSW: Levantine Surface Water; LIW: Levantine Intermediate Water; TMW: Transitional Mediterranean Water; EMDW: East Mediterranean Deep Water; CDW: Cretan Deep Water.

	Potential temperature (°C)	Salinity	Dissolved oxygen (μM)	Phosphate (μM)	Nitrate + nitrite (μM)	Silicate (μM)	Mass conservation	Method[a]
AW-SC	17.70	37.38	234.08	0.06	0.22	0.89	1	1
AW	23.29	38.10	223.65	0.02	0.40	0.77	1	2
LSW	24.03	39.36	215.76	0.02	0.20	0.85	1	3
LIW	14.36	38.88	203.08	0.18	4.10	5.80	1	4
TMW	13.64	38.76	190.80	0.21	5.16	10.46	1	5
EMDW	13.49	38.75	209.04	0.17	3.51	6.11	1	6
CDW	13.66	38.80	199.87	0.19	4.53	9.75	1	7
Weights	25	25	7	4	7	7	25	8

[a] Method 1 – Average (Avg) of the June 2004 and June 2006 data collected in the Sicily Channel; 2 – End member at V06 (the parameters corresponding to the sample with minimum salinity); 3 – End member at V10 (the parameters corresponding to the sample with maximum salinity); 4 – Avg of the layer between 200 and 750 m at V07, V08, and V10; between 400 and 750 m at V09; 5 – Avg in the layer between 1000 and 1500 m at V09, and between 750 and 1500 m at V10; 6 – Avg of the layer between 2250 and 2350 m at V06; 7 – Avg of the layer between 2000 and 3400 m at V10; 8 – see Section 3.5.

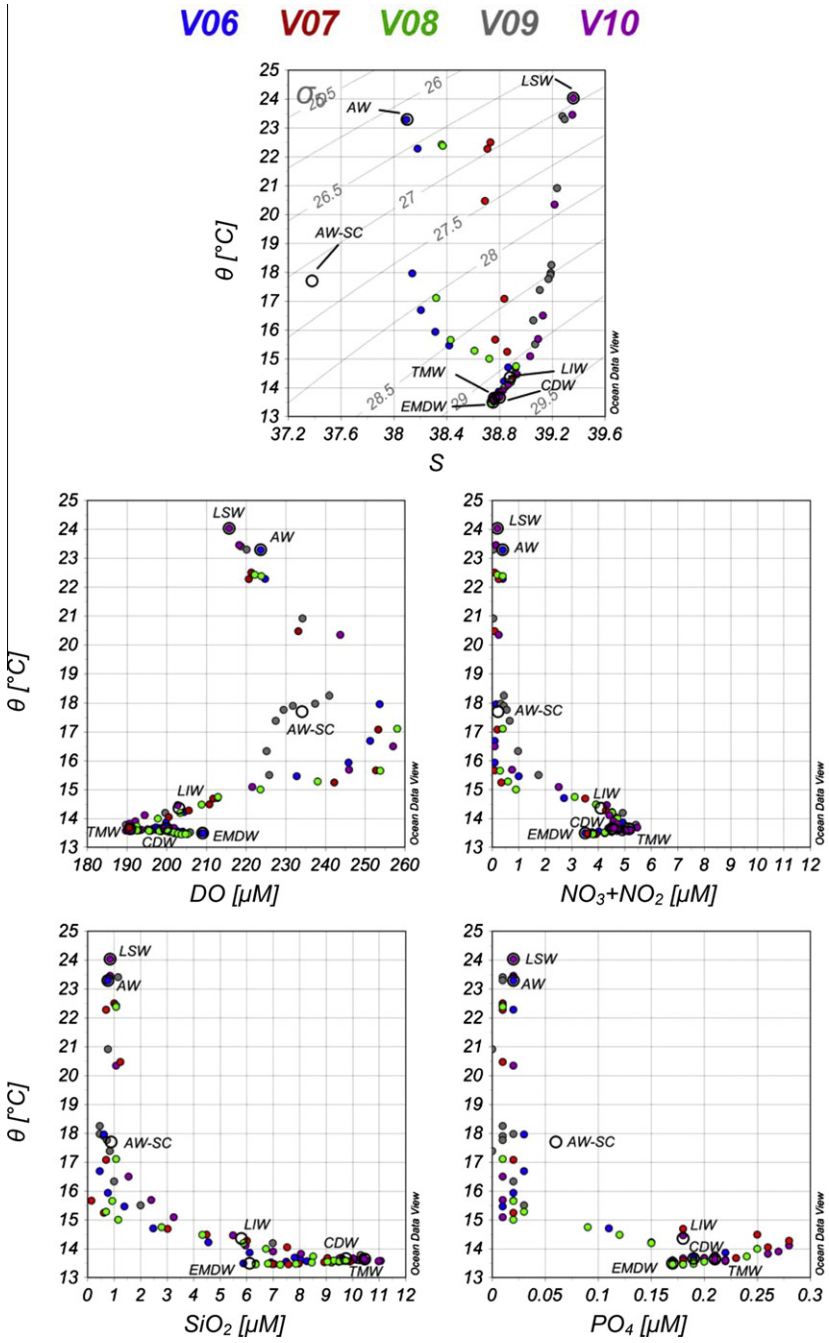

Fig. 10. Property–property plots corresponding to the water samples (coloured dots) and characteristic values of the water masses for the OMP analysis from Table 1 (open circle): (a) θ–S diagram from the chemical casts with values at sampling depths; (b) θ versus dissolved oxygen; (c) θ versus dissolved nitrate + nitrite; (d) θ versus dissolved silicate; (e) θ versus dissolved phosphate. AW–SC stands for the Atlantic Water–Sicily Channel. Labelled grey dashed lines are density isolines of σ_0 (kg/m^3). Colour code refers to the stations.

towards the west from its source regions (one could be near V10) where its formation typically occurs during winter by cooling of the salty surface waters, their sinking in the eastern Levantine (Özsoy et al., 1993; Malanotte-Rizzoli et al., 1999) and possible trapping within the Ierapetra ACG.

TMW prevailed in the eastern part of the basin between 500 and 2000 m (60–90%), while at V06 its fraction was about 50% in the layer around 1000 m depth (Fig. 11). The increased depth of its core at V09 is again the signature of downwelling within the Ierapetra ACG.

EMDW was present with a fraction of 90% in the bottom layer at V06 and to a lesser extent at V07 and V08 (Fig. 12). Varying proportions of the EMDW both horizontally and vertically could indicate a different age and/or different thermohaline properties (density) of the EMDW on its course towards the east. The actual EMDW is a composition of thermohaline properties due to the diverse contributions of the AdDW (Cardin et al., 2011) after receiving a considerable amount of the Aegean waters (CDW) reversed during the EMT (Roether et al., 2007).

CDW was abundant (80–90%) in the deep layer (>2500 m) at V10 (Fig. 12). This was probably the oldest remnant of its densest overflow across the Kasos Strait during the EMT (Roether et al., 2007). It was less abundant (70–80%) in the deep layer (>3000 m) at V09. A small fraction of it (10–20%) occupied the lay-

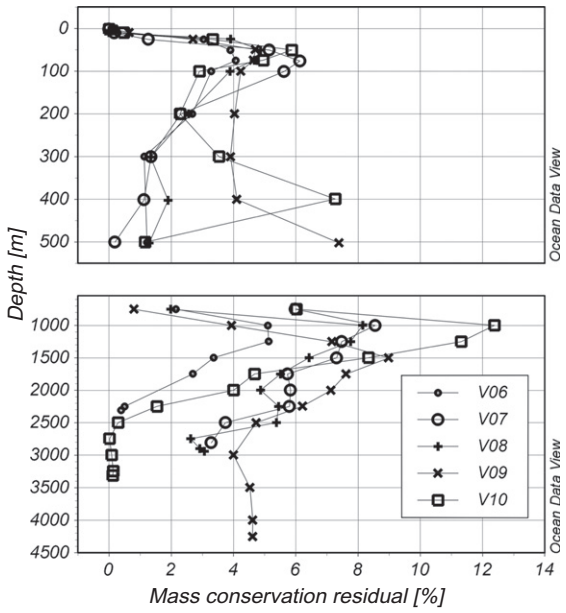

Fig. 11. Mass conservation residuals (%) versus depth.

ers 1000–2000 m at V07 and V08. CDW was almost absent at V06. Such a distribution might be a consequence of the CDW spreading mainly around the Cretan Arc Straits. As Roether et al. (2007) observed, until 1995 its signature was fading along the northern and western periphery of the Ionian Sea, where it entered at the western end of the Eastern Mediterranean Ridge. At V07 and V08 there might actually be influence from a less dense Aegean water (maybe CIW), probably also through the Antikithira Strait (Roether et al., 2007), which was not taken into account in our analysis and which leaks into the properties of the CDW at these two stations. In addition, Manca et al. (2006) observed that by 2002 the greatest depths in the central and western Ionian were filled predominantly by EMDW, while CDW was observed at the mid-depths.

An area of about 100 km^2 to the north of the station V06, in the northern Ionian, was investigated by Budillon et al. (2010) during 2004–2006. In that area the maximum depth is about 1400 m. We detected some analogies in the vertical distribution of the water masses, even though with somewhat different properties than those encountered at V06 in 2007. Budillon et al. (2010) found that the AW together with the Ionian Surface Water (which we do not consider in our analysis) dominated the surface layers. At greater depth, the composition of the water column was mostly due to the presence of the LIW (with maximum contribution at about 200 m), of the TMW (with a variable contribution in the

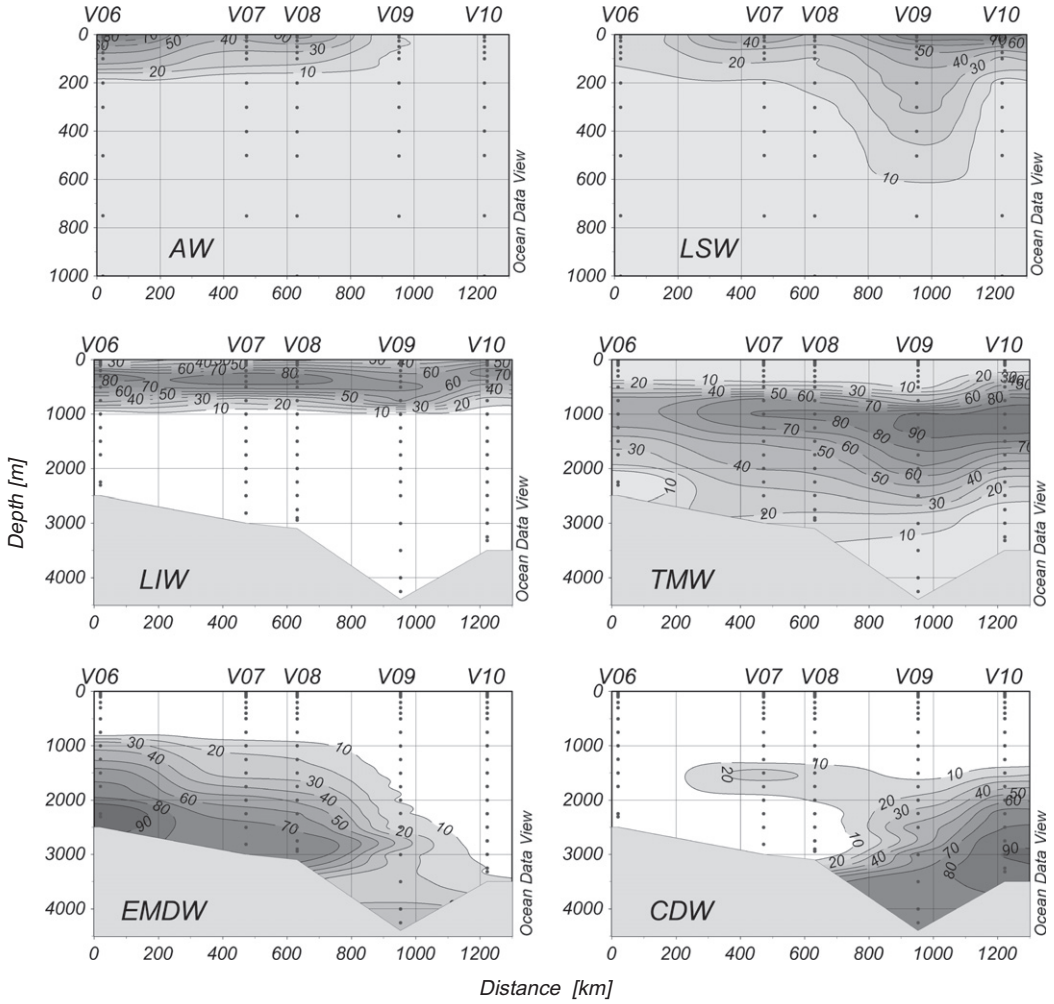

Fig. 12. Mixing fractions (%) at sampling depths of the principal EMED water masses: AW, LSW, LIW, TMW, EMDW and CDW. AW: Atlantic Water; LSW: Levantine Surface Water; LIW: Levantine Intermediate Water; TMW: Transitional Mediterranean Water; EMDW: East Mediterranean Deep Water; CDW: Cretan Deep Water.

layer 400–800 m), and of the occasional signature and relatively low contribution of the CDW between 500 and 1000 m. They observed a clear signature of the AdDW flowing westward in the bottom layer, away from the Strait of Otranto which is about 60 km distant. This is one of the possible spreading paths in the Ionian Sea when AdDW is not dense enough to descend and mix to form the EMDW in the deepest region of the Ionian Sea, in contrast to what was observed by Manca et al. (2003).

3.7. Comparison with historical data

The prevailing conditions at the five locations of the EMED in June 2007 are compared with the available past observational studies conducted in close proximity. At some locations we were able to follow the evolution in time after 2007, thanks to the availability of post-2007 data (Hainbucher, 2009, 2010; Bensi et al., personal communication).

The stations of our cruise in June 2007 were located in the EMED regions where, in the early 90s, significant effects of the EMT were observed down the water column (Roether et al., 2007, and references therein). Relatively frequent *in situ* measurements since then allowed description of the evolution of the thermohaline properties, comparing the states of the pre- and post-EMT periods. In particular, Roether et al. (2007) thoroughly dealt with the observed variability in each sub-basin of the EMED and detailed the temporal evolution of the EMT until 2002. Moreover, they established the pathways and the time scales of dispersion of the CDW.

One of the most salient issues, the feedback of the EMT on the AdDW production and its properties, is discussed in Klein et al. (2000). They showed the post-EMT phase until 1999 during which the recovery of the southern Adriatic Sea in producing dense waters that ventilated the EMED was evident. They demonstrated that the southern Adriatic Sea has again been involved in producing dense waters, although with different properties (warmer and saltier) than before EMT. Manca et al. (2003) studied in great detail the prevailing conditions of the EMED based on basin-wide data collected in 1999. They also showed the temporal fluctuations in the characteristic θ–S properties during the period 1986–1999 in the Strait of Otranto and in the southern Adriatic related to AdDW and LIW. These water masses play essential roles in the formation of the dense waters of the EMED. A comprehensive analysis of the southern Adriatic and the Ionian Sea from the hydrographic data collected in 2002 is given in Manca et al. (2006). They established that the greatest depths in the central and western Ionian were filled predominantly by EMDW, while CDW retreated to the mid-depth. The most recent update of the winter convection processes and the thermohaline properties of the southern Adriatic are described by Civitarese et al. (2005) for the period 1997–2005 and by Cardin et al. (2011) for the period 2006–2009. In the latter paper, the authors draw attention to the decadal variability of the average thermohaline properties of the 200- to 1000-m layer in the southern Adriatic, within which the AdDW is formed and spread over the sill in the Strait of Otranto further into the Ionain Sea. They found that, after the EMT, the intermediate-layer properties essentially underwent three phases: (1) σ_0 decrease (<29.20 kg/m^3) with significant θ and S increases (13.20–13.60 °C and 38.64–38.80, respectively) during 1995–2003; (2) σ_0 increase up to the maximum (>29.20 kg/m^3) maintaining high θ (13.50–13.60 °C) and increasing S (38.68–38.79) during 2004–2006; (3) a tendency to a slightly lower S (38.72–38.76) and lower θ (13.40–13.55 °C), associated with a final σ_0 of about 29.20 after 2006. All this variability affects the properties of the most recent EMDW.

The evolution of the thermohaline properties until and after 2007 is presented as θ, S and σ_{2000} vertical profiles. The individual profiles in the vicinity of the five stations are examined. Even though the full-depth profiles are presented, the discussion focuses on the intermediate, mid-depth and deep layers of the water column because in the upper 500 m the variability of the θ–S properties is high, due to different factors such as seasonality and the influence of subbasin gyres and eddies. Density σ_{2000} was chosen in order to avoid unrealistic instability and differences in density of the deep waters with different θ and S properties. However, σ_{2000} and σ_{3000} (the latter is the quantity used by Roether et al. (2007), when comparing the bottom waters) were compared, and the differences between these two variables did not influence the qualitative judgment. Therefore we continued to use σ_{2000}, bearing in mind that our primary discussion is of qualitative character. The profiles of θ and S from 1987 are regarded as a pre-EMT state.

The chronological evolution for the northern Ionian Sea was reconstructed around the station V06 (Fig 13). In 1987, properties of the deep layer consistently indicated what was known as EMDW, with characteristic low θ–S (~13.23 °C, 38.66), influenced by the AdDW (Malanotte-Rizzoli et al., 1999). In 1995, considered an early post-EMT period, the deep layers were replenished by saltier (thus denser) waters originating in the Aegean Sea (Roether et al., 1996), but the layers at about 1000 m were less salty and less warm than in 1987, explained by the upward displacement of the old deep waters (Roether et al., 1996). In 2002 the deep layers were even saltier and warmer than in 1995, suggesting a time-lag in propagation of the EMT signal toward this part of the northern Ionian. At the same time a salinity maximum at about 500 m indicated the presence of waters saltier and deeper than usually observed at the traditional LIW horizon (200–300 m). The 2007 state around 1000 m depth and near the bottom (at about 2500 m) resembled that of 2002. The layer between these two in 2007 was cooler and fresher than in 2002. The same tendency was observed in 2009 below 2000 m. However, on the whole, deep waters were still warmer and saltier than before the EMT. As far as the densities of the deep waters are concerned, they were all within 0.005 kg/m^3 in terms of σ_{2000}. Values of σ_{2000} in 1995 and 2002 were, however, higher, while σ_{2000} values in 2007 and 2009 were lower than the one in 1987.

In the western Ionian Sea, the profiles for a comparison were scattered more than 0.5° in latitude or longitude around the station V07 (Fig. 14). Below 1000 m after 1999, when the highest θ and S were observed, θ and S were decreasing. Nevertheless, in 2007 they were still higher then during the pre-EMT period (1987). This could be a consequence of a gradual mixing of the waters discharged during the EMT from the Aegean Sea with the recentmost intrusion of the dense waters of the Adriatic origin, as put forward by Roether et al. (2007).

In the deep waters (>1000 m) of the western Cretan Passage, where station V08 is located (Fig. 15), the most characteristic feature was a continous decrease in θ and S until 2007, detected after the maximum observed in 1995 (early post-EMT). Afterwards, in 2009 and 2010 this trend seemed to be arrested and the deep layer (below 2500 m) was more uniform, especially in salinity. As stated by Roether et al. (2007), this decrease is a consequence of the mixing of the dense waters of south Aegean Sea origin spreading westward along the Hellenic Trench with the less saline and colder EMDW of Adriatic origin spreading eastward, probably at greater depths. In the near bottom layers (at about 3000 m), densities in 2007, 2009 and 2010 were similar to and lower than in 1995 and 2001.

In the eastern Cretan Passage near station V09 (Fig. 16), a rather similar decline from the maximum θ–S values in 1995 was detected below 1500 m. In particular, the bottom 13.84 °C and 38.87 were reduced to 13.5 °C and 38.75 in 2007.

In the eastern Levantine basin, at the northern edge of the Rhodos CG, where station V10 is located (Fig. 17), the history of the θ–S properties indicates that the largest EMT signature was in 1995,

with a marked double θ–S peak below 1000 m. The deepest one was due to the dense waters of Aegean Sea origin that replaced the earlier EMDW of lower θ–S. In 2007 there was no evidence of the double θ–S peak. Instead, a local θ–S minimum at around 1000 m, a constant rise down to 2400 m, and a uniform bottom layer might be evidence of a further mixing within the deep water

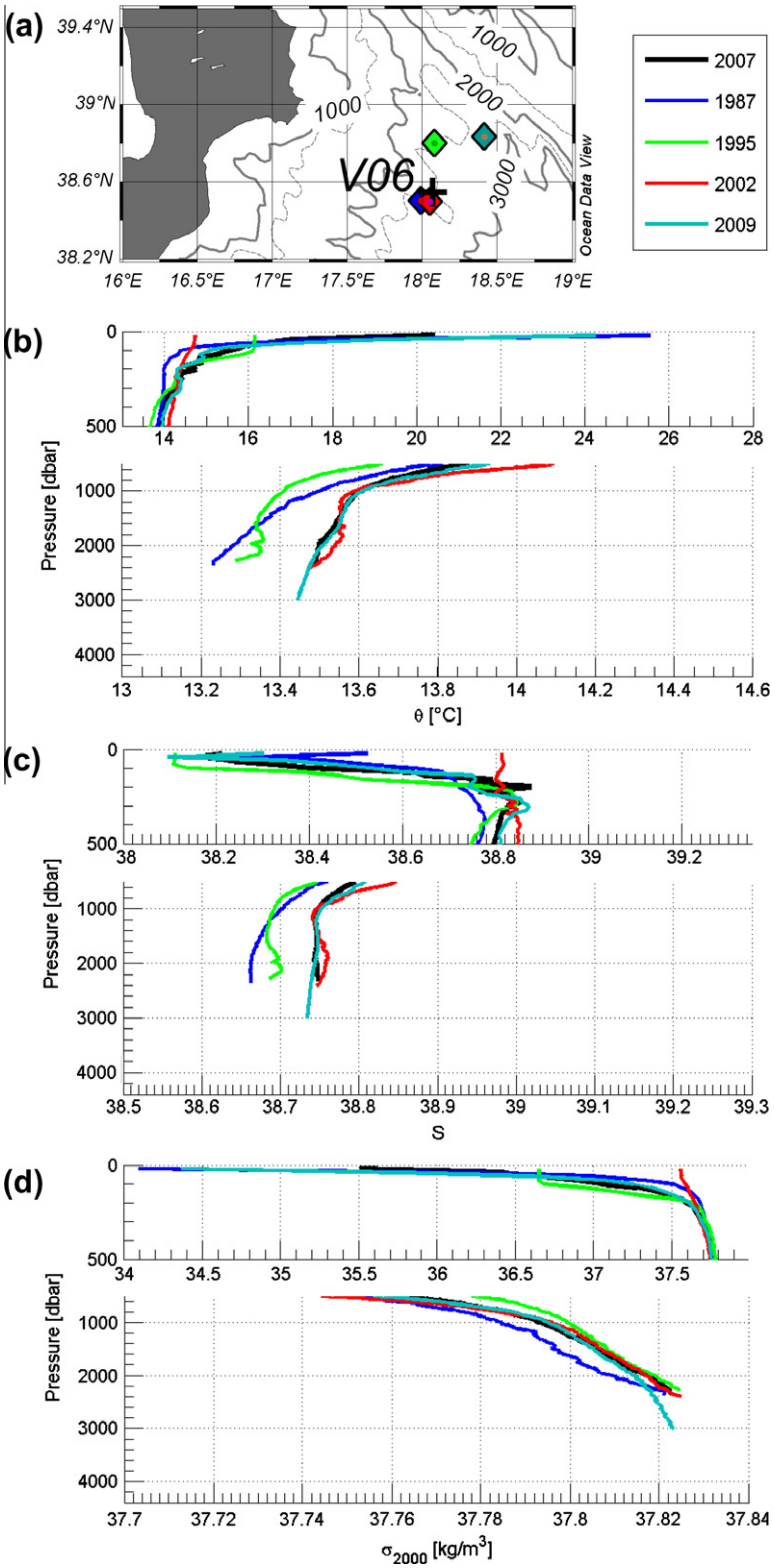

Fig. 13. Comparison of the thermohaline properties in the northern Ionian Sea (V06) in 2007 (black line and cross) with other profiles (colour-coded lines and diamonds) observed in 1987 (7 September 1987; POEM05-AS87 OGS-I cruise), in 1995 (15 January 1995; POEM-BC-LIWEX 95 cruise), in 2002 (4 April 2002; S402 cruise) and in 2009 (8 October 2009, MSM 13/2 cruise). (a) Location and year of the profiles; (b) potential temperature referenced to 0 dbar; (c) salinity; (d) density in terms of σ_{2000}. Dashed grey bathymetric contours in (a) are plotted for 1500 and 2500 m.

column. In 2007, the bottom values, 13.65 °C and 38.8, were lower than in 1995 but still appreciably higher than in 1987. The deep densities were similar in 1995 and 2007, and higher than in 1987.

4. Summary and conclusions

The oceanographic cruise in June 2007 in the EMED had the aim of characterizing the dynamics and the physical properties down

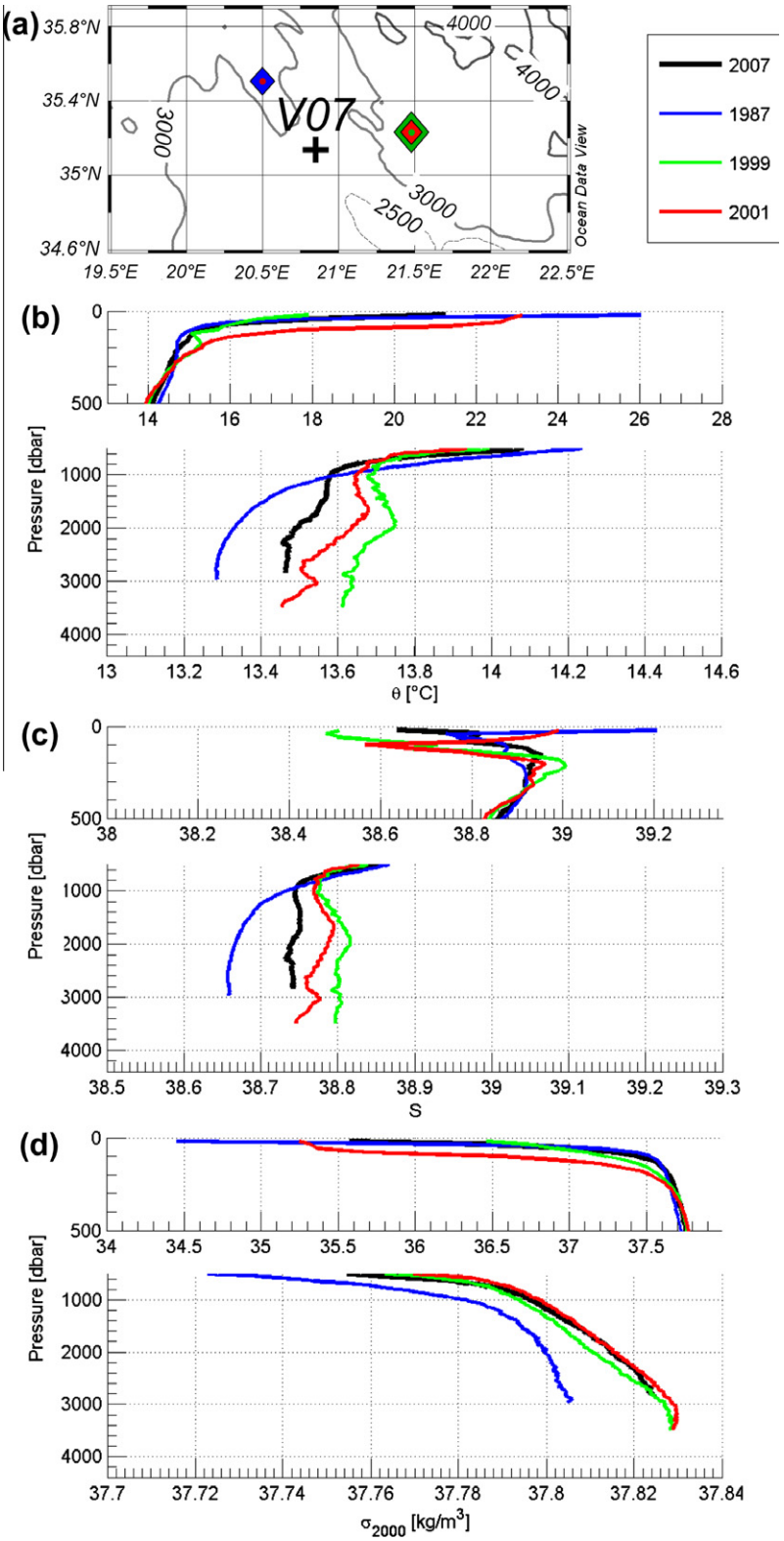

Fig. 14. Comparison of the thermohaline properties in the western Ionian Sea (V07) in 2007 (black line and cross) with other profiles (colour-coded lines and diamonds) observed in 1987 (4 September 1987; POEM05-AS87 OGS-I), in 1999 (7 May 1999; ME99) and in 2001 (25 October 2001; ME01 cruise). (a) Location and year of the profiles; (b) potential temperature referenced to 0 dbar; (c) salinity; (d) density in terms of σ_{2000}.

the water column at five locations, as well as to provide a physical framework useful for the definition of the biogeochemical processes responsible for the marine carbon cycle (sequestration and release). The five study areas were located in the northern and in the eastern Ionian Sea, in the western Cretan Passage, in the zone of the Ierapetra ACG and at the northern border of the Rhodos

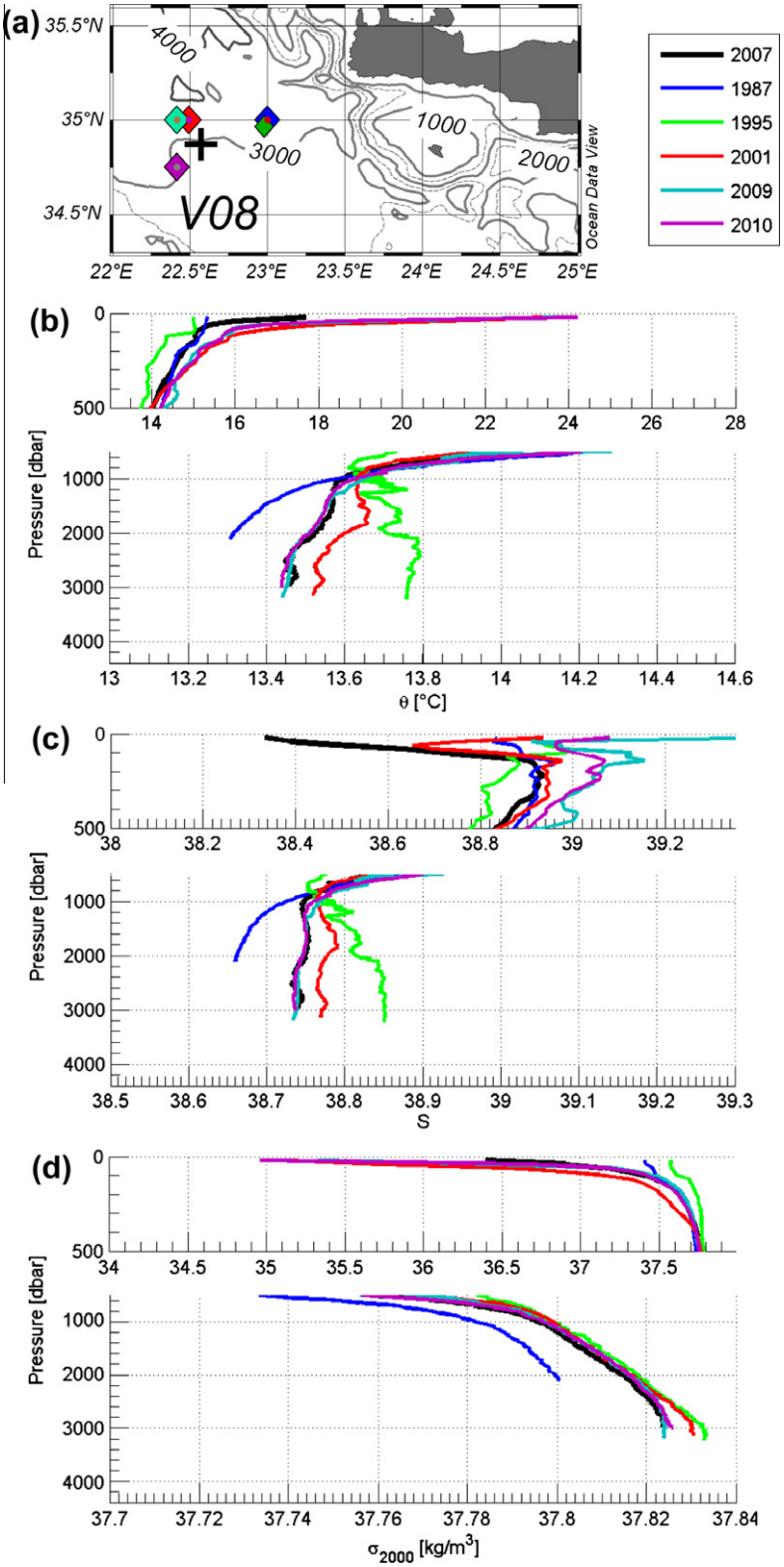

Fig. 15. Comparison of the thermohaline properties in the western Cretan Passage (V08) in 2007 (black line and cross) with other profiles (colour-coded lines and diamonds) observed in 1987 (2 May 1987; POEM-IV-87 LIA5 cruise), in 1995 (21 January 1995; POEM-BC-LIWEX cruise), in 2001 (25 October 2001, ME01 cruise), in 2009 (19 October 2009, MSM 13/2 cruise) and in 2010 (14 July 2010, MSM 15/4 cruise). (a) Location and year of the profiles; (b) potential temperature referenced to 0 dbar; (c) salinity; (d) density in terms of of σ_{2000}. Dashed grey bathymetric contours in (a) are plotted for 1500 and 2500 m.

CG. Each of these areas has its particular characteristics that possibly drive differently the cycling of organic and inorganic carbon.

The map of the absolute dyanamic topography shows the presence of subbasin and mesoscale dynamic structures that are superimposed on the general basin-scale circulation. They are supported by the features observed in the SST and surface chlorophyll-*a* concentrations.

The water column properties are influenced by the permanent mesoscale dynamic structures, such as Ierapetra ACG. This determines the homogenisation and vertical downward transfer of sur-

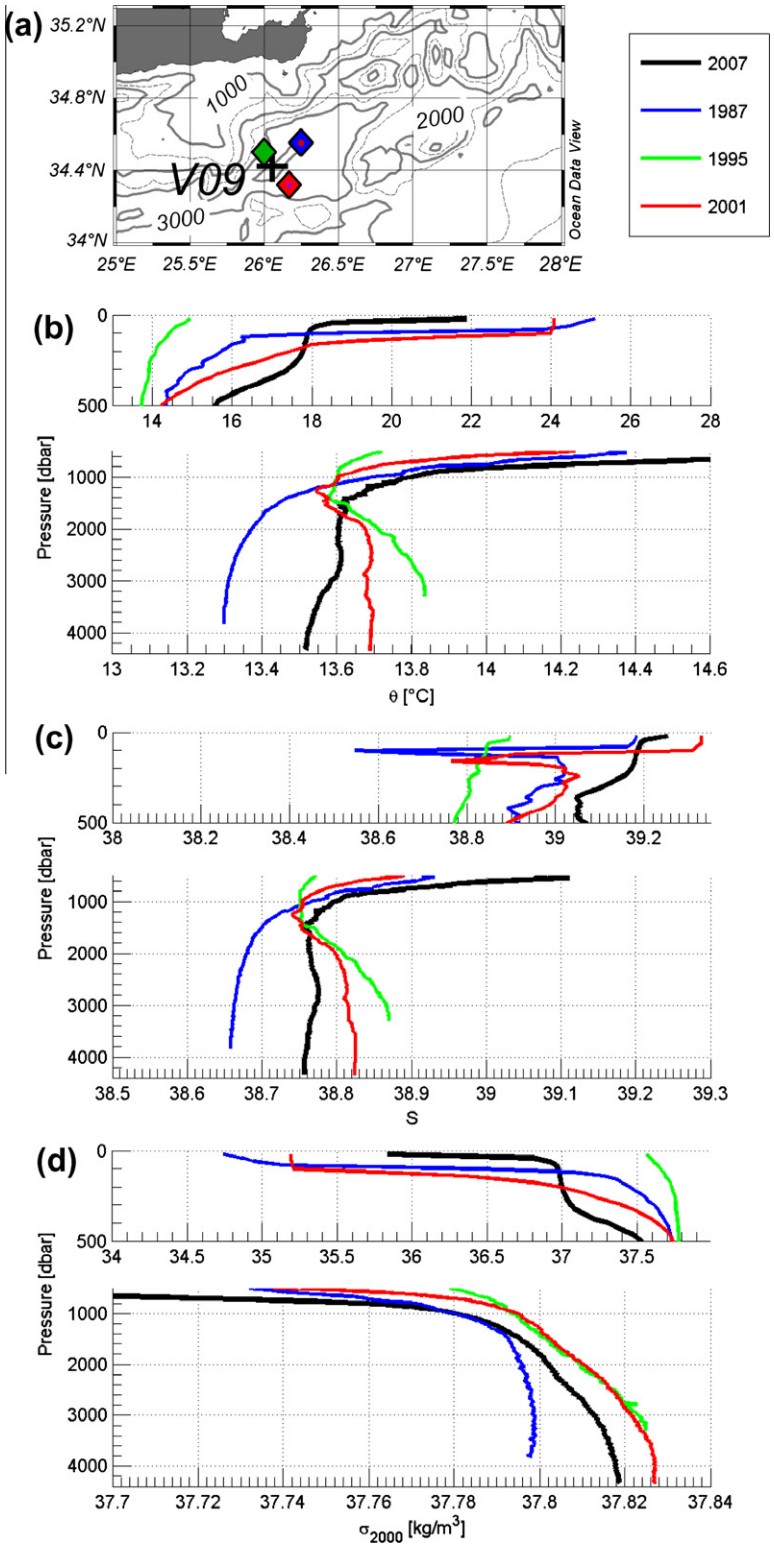

Fig. 16. Comparison of the thermohaline properties in the eastern Cretan Passage (V09) in 2007 (black line and cross) with other profiles (colour-coded lines and diamonds) observed in 1987 (30 August 1987; POEM05-AS87-OGS cruise), in 1995 (24 January 1995; POEM-BC-LIWEX 95 cruise) and in 2001 (30 October 2001; ME01 cruise). (a) Location and year of the profiles; (b) potential temperature referenced to 0 dbar; (c) salinity; (d) density in terms of σ_{2000}. Dashed grey bathymetric contours in (a) are plotted for 1500 and 2500 m.

face properties to great depths (1000 m), whereas some other locations are influenced predominantly by advective processes, for instance at the border of structures such as the Rhodos CG.

In the upper layer, influenced by the seasonal thermocline, a general increasing trend of temperature and salinity from west to east was evident. Moreover, the surface properties varied due to the presence of horizontal fronts that separate the observed dynamic structures and show their signatures down to 200–300 m.

A gradual propagation of AW was traced from a drifter trajectory, which indicates its spreading from the Sicily Channel in an anticyclonic sense around the Ionian Sea, towards the Cretan Passage. This feature is consistent with the findings of Gačić et al.

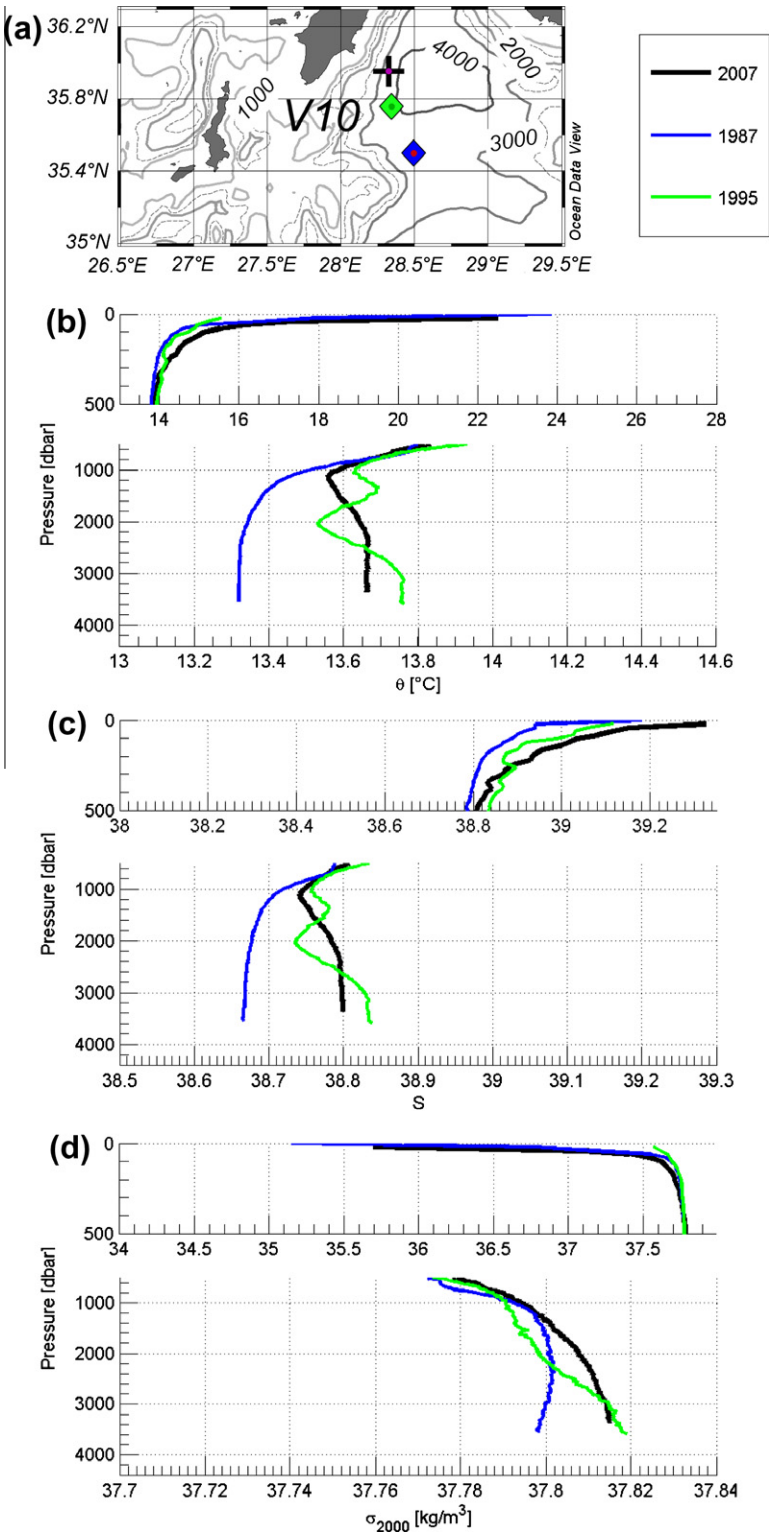

Fig. 17. Comparison of the thermohaline properties in the eastern Levantine basin (V10) in 2007 (black line and cross) with other profiles (colour-coded lines and diamonds) observed in 1987 (20 August 1987; POEM05-AS-87 OGS cruise) and in 1995 (29 January 1995; POEM-BC-LIWEX 95 cruise). (a) Location and year of the profiles; (b) potential temperature referenced to 0 dbar; (c) salinity; (d) density in terms of σ_{2000}. Dashed grey bathymetric contours in (a) are plotted for 1500 and 2500 m.

(2010), who claim that, as a consequence of decadal oscillations in the upper layer circulation in the northwestern Ionian, the inversion from the cyclonic to the anticyclonic one occurred in 2006. According to these authors, this type of circulation regime favours the spreading of the AW toward the northern Ionian and further into the southern Adriatic. The opposite is the case of the cyclonic regime, which obstructs the AW spreading but favours the salty intermediate waters spreading from the Levantine/south Aegean to reach the northern Ionian and, hence, the Adriatic Sea. This fact is important because it might have direct consequences for the density of the AdDW formed in the southern Adriatic Sea (e.g., Klein et al., 2000), and thus on its outflow and spreading into the Ionian. An ultimate effect of varying properties of the AdDW is its influence on the EMDW. We assumed that temperature, salinity and density of the EMDW observed in June 2007 at locations in the Ionian Sea were the result of all those different contributions of the preceeding AdDW formation and of spreading and mixing processes.

The signature of the saltier and warmer LSW gradually vanished from east to west. In the intermediate layers (200–500 m) the westward propagation of the high-salinity signal is attributed to the LIW. At greater depth, between about 600 and 1500 m, the TMW signal gradually attenuates as it mixes with the surrounding waters. The deep and bottom layers are characterized by the EMDW signal in the northern and eastern Ionian, while in the Levantine basin the influence of the EMT overflow of the saline and warm CDW is still evident.

The θ–S properties in June 2007 almost entirely show a continous relaxation of the EMT since the early 1990s. In 2007 the deep waters of the EMED in the western Cretan Passage and in the western Ionian had the lowest θ–S since the relaxation began. At the former location the recently observed properties (in 2009 and 2010) are also similar to those in 2007, but higher than before the EMT (Sparnocchia et al., 2011; Bensi et al., personal communication). Only in the northern Ionian Sea was the maximum signature of the EMT in the deep layers observed, not in 1995 but in 2002 (due to the time lag of the EMT signal spreading northward and westward from the Hellenic Trench; Roether et al., 2007). There the bottom θ values in 2007, as well as in 2009, were similar to those found in 2002, while S values seemed to decline further in 2009.

As investigated by Roether et al. (2007) until 2001, the near-linear relationship between θ and S of the deep water in various areas of the EMED is a sign of mixing, horizontally and vertically, and of entrainment of the different waters into the Aegean overflow. These processes, apparently less vigorous, seemed to be still active in 2007.

Acknowledgements

The VECTOR project was funded by the Italian Ministry of Education, University and Research (MIUR), Ministry of Economy and Finance, Ministry of Ambient and Safeguarding of the Territory, and Ministry of Agricultural and Forestry Politics, through the Integrated Special Fund for the Research (FISR in 2001). The authors thank the captain and the crew of the R/V Universitatis for their competent support in the sea operations. The help and expertise in OMP analysis of Massimo Pacciaroni (OGS) were greatly appreciated. The altimeter products (downloaded ADT data) were produced by SSALTO/DUACS (Segment Sol multimissions d'ALTimétrie, d'Orbitographie et de localisation precise/Data Unification and Altimeter Combination System) and distributed by AVISO (Archiving, Validation and Interpretation of Satellite Oceanographic data), with support from CNES (Centre National d'Études Spatiales) (http://www.aviso.oceanobs.com/duacs/). The Mediterranean Argo database used for the work presented in this paper was downloaded from the Argo Global Data Assembly Center (GDAC; http://www.coriolis.eu.org/) in June 2009. We also acknowledge NODC-OGS (National Oceanographic Data Center/IOC of OGS) for CTD data profiles used for the historical comparison, and appreciate the effort of all Italian and international institutions that have collaborated in the population of this data bank. Constructive comments from the anonymous reviewer were highly appreciated and helpful in improving the manuscript. The authors received a partial funding from the Italian national scientific research programme RITMARE (La Ricerca ITaliana per il MARE).

References

Bensi, M., Hainbucher, D., Cardin, V., Mancero-Mosquera, I., Rubino, A., personal communication. Structure and Variability of the Abyssal Water Masses of the Ionian Sea in the Period 2009–2010: Their Links with the Adriatic and Aegean Sea.

Beuvier, J., Sevault, F., Herrmann, M., Kontoyiannis, H., Ludwig, W., Rixen, M., Stanev, E., Beranger, K., Somot, S., http://dx.doi.org/10.1029/2009JC005950, 2010. Modelling the Mediterranean Sea interannual variability during 1961–2000: focus on the Eastern Mediterranean Transient. Journal of Geophysical Research 115, C08017.

Budillon, G., Lo Bue, N., Siena, G., Spezie, G., 2010. Hydrographic characteristics of water masses and circulation in the Northern Ionian Sea. Deep-Sea Research II 57, 441–457.

Candela, J., Beardslay, R.C., Limeburner, R., 1992. Separation of tidal and subtidal currents in ship-mounted Acoustic Doppler Current Profiler observations. Journal of Geophysical Research 97 (C1), 769–788.

Cardin, V., Bensi, M., Pacciaroni, M., http://dx.doi.org/10.1016/j.csr.2011.03.002, 2011. Variability of water mass properties in the last two decades in the South Adriatic Sea with emphasis on the period 2006–2009. Continental Shelf Research.

CIESM, 2008. Impacts of acidification on biological, chemical and physical systems in the Mediterranean and Black Seas. In: Briand, F. (Ed.), CIESM Workshop Monographs, No. 36, Monaco, 124 p.

Civitarese, G., Gacic, M., Cardin, V., Ibello, V., 2005. Winter convection continues in the warming Southern Adriatic. Eos 86, 445–451.

D'Ortenzio, F., Ribera D'Alcalà, M., 2009. On the trophic regimes of the Mediterranean Sea: a satellite analysis. Biogeosciences 6, 139–148.

Gačić, M., Borzelli, G.L.E., Civitarese, G., Cardin, V., Yari, S., http://dx.doi.org/10.1029/2010GL043216, 2010. Can internal processes sustain reversals of the ocean upper circulation? The Ionian Sea example. Geophysical Research Letters 37, L09608.

Gerin, R., Poulain, P.-M., Taupier-Letage, I., Millot, C., Ben Ismail, S., Sammari, C., 2009. Surface circulation in the Eastern Mediterranean using Lagrangian drifters (2005–2007). Ocean Science 5, 559–574.

Grasshoff, K., 1983. Determination of oxygen. In: Grasshoff, K., Ehrhardt, M., Kremling, K. (Eds.), Methods of Seawater Analysis. Verlag Chemie GmbH, Weinheim, pp. 61–72.

Hainbucher, D., 2009. Dynamic Processes in the Deep Eastern Mediterranean: Deep Water Formation and Energy Sources for Chemosynthetic Ecosystems, Part 1, Cruise No. 13, Leg1-2, FS Maria S. Merian. Institut für Meereskunde, ZMAW, Universität Hamburg, 23 pp.

Hainbucher, D., 2010. Summary Cruise Report RV Maria S. Merian Cruise MSM15/4. Institut für Meereskunde, ZMAW, Universität Hamburg, 9 pp.

Hamad, N., Millot, C., Taupier-Letage, I., 2006. The surface circulation in the eastern basin of the Mediterranean Sea. Scientia Marina 70, 457–503.

Hansen, D.V., Poulain, P.-M., 1996. Processing of WOCE/TOGA drifter data. Journal of Atmospheric and Oceanic Technology 13, 900–909.

Josey, A.S., http://dx.doi.org/10.1029/2003JC001778, 2003. Changes in the heat and freshwater forcing of the Eastern Mediterranean and their influence on deep water formation. Journal of Geophysical Research 108(C7), 3237.

Karstensen, J., Tomczak, M., 1998. Age determination of mixed water masses using CFC and oxygen data. Journal of Geophysical Research 103 (C9), 18,599–18,609.

Karstensen, J., Tomczak, M., 1999. OMP Analysis Package for MATLAB, Version 2.0. <http://www.ldeo.columbia.edu/~jkarsten/omp_std/README.html>.

Klein, B., Roether, W., Manca, B., Bregant, D., Beitzel, V., Kovacevic, V., Luchetta, A., 1999. The large deep transient in the Eastern Mediterranean. Deep-Sea Research I 46, 371–414.

Klein, B., Roether, W., Civitarese, G., Gacic, M., Manca, B.B., Ribera d'Alcalà, M., 2000. Is the Adriatic returning to dominate the production of Eastern Mediterranean Deep Water? Geophysical Research Letters 27, 3377–3380.

Kontoyiannis, H., Theocharis, A., Balopoulos, E., Kioroglou, S., Papadopoulos, V., Collins, M., Velegrakis, A.F., Iona, A., 1999. Water fluxes through the Cretan Arc Straits, Eastern Mediterranean Sea: March 1994 to June 1995. Progress in Oceanography 44, 511–529.

Koroleff, F., Grasshoff, K., 1983. Determination of nutrients. In: Grasshoff, K., Ehrhardt, M., Kremling, K. (Eds.), Methods of Seawater Analysis. Verlag Chemie GmbH, Weinheim, pp. 125–187.

Lascaratos, A., Roether, W., Nittis, K., Klein, B., 1999. Recent changes in deep water formation and spreading in the Mediterranean Sea: a review. Progress in Oceanography 44 (1–3), 5–36.

Lozano, C.J., Candela, J., 1995. The M2 tide in the Mediterranean Sea: dynamic analysis and data assimilation. Oceanologica Acta 18 (4), 419–441.
Mackas, D.L., Denman, K.L., Bennet, A.F., 1987. Least-square multiple tracer analysis of water mass composition. Journal of Geophysical Research 92, 2907–2918.
Malanotte-Rizzoli, P., Manca, B.B., D'Alcalà, M.R., Theocharis, A., Bergamasco, A., Bregant, D., Budillon, G., Civitarese, G., Georgopoulos, D., Michelato, A., Sansone, E., Scarazzato, P., Souvermezoglou, E., 1997. A synthesis of the Ionian Sea hydrography, circulation and water mass pathways during POEM-Phase I. Progress in Oceanography 39, 153–204.
Malanotte-Rizzoli, P., Manca, B.B., D'Alcalà, M.R., Theocharis, A., Brenner, S., Budillon, G., Ozsoy, E., 1999. The Eastern Mediterranean in the 80s and in the 90s: the big transition in the intermediate and deep circulations. Dynamics of Atmospheres and Oceans 29, 365–395.
Manca, B.B., Budillon., G., Scarazzato, P., Ursella, L., http://dx.doi.org/10.1029/2002JC001664, 2003. Evolution of dynamics in the eastern Mediterranean affecting water mass structures and properties in the Ionian and Adriatic Seas. Journal of Geophysical Research 108(C9), 8102.
Manca, B.B., Ibello, V., Pacciaroni, M., Scarazzato, P., Giorgetti, A., 2006. Ventilation of deep waters in the Adriatic and Ionian Seas following changes in thermohaline circulation of the Eastern Mediterrranean. Climatic Research 31, 239–256.
Mann, K.H., Lazier, J.R.N., 1991. Dynamics of Marine Ecosystems: Biological–Physical Interactions in the Oceans. Blackwell Scientific Publications, Inc., Boston, 466 pp.
Nair, R., Medeot, N., 2007. Test Report. SBE 911plus CTD – Temperature and Conductivity Sensor Modules. SBE 3 Temperature Sensor s/n 1709. SBE 4 Conductivity Sensor s/n 1487. SBE 3 Temperature Sensor s/n 1717. SBE 4 Conductivity Sensor s/n 1489. Property of: Istituto Nazionale di Oceanografia e di Geofisica Sperimentale – OGS, Trieste, Department of Oceanography. Rapporto tecnico, Istituto Nazionale di Oceanografia e di Geofisica Sperimentale – OGS, REL. 2007/83 OGA 25 CTO, Borgo Grotta Gigante (TS), 15 November 2007.
Nittis, K., Pinardi, N., Lascaratos, A., 1993. Characteristics of the summer 1987 flow field in the Ionian Sea. Journal of Geophysical Research 98 (C6), 10171–10184.
Notarstefano, G., Poulain, P.-M., 2009. Thermohaline Variability in the Mediterranean and Black Seas as Observed by Argo Floats in 2000–2009. OGS Tech. Rep. OGS 2009/121 OGS 26 SIRE, Trieste, Italy, 72 pp.
Özsoy, E., Hecht, A., Ünlüata, Ü., Brenner, S., Sur, H.İ., Bishop, J., Latif, M.A., Rosentraub, Z., Oğuz, T., 1993. A synthesis of the Levantine Basin circulation and hydrography, 1985–1990. Deep-Sea Research II 40 (6), 1075–1119.
The POEM Group, 1992. General circulation of the Eastern Mediterranean. Earth-Science Review 32, 285–309.
Poulain, P.-M., Barbanti, R., Cecco, R., Fayes, C., Mauri, E., Ursella, L., Zanasca, P., 2004. Mediterranean Surface Drifter Database: 2 June 1986 to 11 November 1999, Rel. 75/2004/OGA/31, OGS, Trieste, Italy. <http://poseidon.ogs.trieste.it/drifter/database_med> (CDRom and Online Dataset).
Poulain, P.-M., Barbanti, R., Font, J., Cruzado, A., Millot, C., Gertman, I., Griffa, A., Molcard, A., Rupolo, V., Le Bras, S., Petit de la Villeon, L., 2007. MedArgo: a drifting profiler program in the Mediterranean Sea. Ocean Science 3, 379–395.
Poulain, P.-M., Gerin, R., Mauri, E., Pennel, R., 2009a. Wind effects on drogued and undrogued drifters in the Eastern Mediterranean. Journal of Atmospheric and Oceanic Technology 26, 1144–1156.
Poulain, P.-M., Solari, M., 2009. Assessment of the Argo sampling in the Mediterranean and Black Seas (Part I) OGS 2009/117 OGA 23 SIRE. Trieste, Italy, 19 pp.
Poulain, P.-M., Solari, M., Notarstefano, G., Ruolo, V., 2009b. Assessment of the Argo Sampling in the Mediterranean and Black Seas (Part II) OGS 2009/139 OGA 32 SIRE. Trieste, Italy, 23 pp.
Robinson, A.R., Golnaraghi, M., Leslie, W.G., Artegiani, A., Hecht, A., Lazzoni, E., Michelato, A., Sansone, E., Theocharis, A., Ünlüata, Ü., 1991. The eastern Mediterranean general circulation:features, structure and variability. Dynamics of Atmospheres and Oceans 15, 215–240.
Roether, W., Manca, B., Klein, B., Bregant, D., Georgopoulos, D., Beitzel, V., Kovacevic, V., Luchetta, A., 1996. Recent changes in Eastern Mediterranean deep waters. Science 271, 333–335.
Roether, W., Klein, B., Manca, B.B., Theocharis, A., Kioroglou, S., 2007. Transient Eastern Mediterranean deep waters in response to the massive dense-water output of the Aegean Sea in the 1990s. Progress in Oceanography 74, 540–571.
Schlitzer, R., 2011. Ocean Data View. <http://odv.awi.de>.
Schroeder, K., Borghini, M., Cerrati, G., Difesa, V., Delfanti, R., Santinelli, C., Gasparini, G.P., 2008. Multiparametric mixing analysis of the deep waters in the Western Mediterranean Sea. Chemistry and Ecology 24 (1), 47–56.
Sparnocchia, S., Gasparini, G.P., Schroeder, K., Borghini, M., http://dx.doi.org/10.1016/j.nima.2010.06.231, 2011. Oceanographic conditions in the NEMO region during KM3NeT project (April 2006–May 2009). Nuclear Instruments and Methods A.
Theocharis, A., Georgopoulos, D., Lascaratos, A., Nittis, K., 1993. Water masses and circulation in the central region of the Eastern Mediterranean: Eastern Ionian, South Aegean and Northwest Levantine, 1986–1987. Deep-Sea Research II 40 (6), 1121–1142.
Theocharis, A., Balopoulos, E., Kioroglou, S., Kontoyiannis, H., Iona, A., 1999. A synthesis of the circulation and hydrography of the South Egean Sea and the Straits of the Cretan Arc (March 1994–January 1995). Progress in Oceanography 44, 469–509.
Tomczak, M., Large, D.G.B., 1989. Optimum multiparameter analysis of mixing in the thermocline of the Eastern Indian Ocean. Journal of Geophysical Research 94 (C11), 16,141–16,149.
Ursella, L., Gacic, M., 2001. Use of the Acoustic Doppler Current Profiler (ADCP) in the study of the circulation of the Adriatic Sea. Annales Geophysicae 19 (9), 1183–1193.
van Aken, H.M., 2000. The hydrography of the mid-latitude northeast Atlantic Ocean I: the deep water masses. Deep-Sea Research I 47, 757–788.
VECTOR, 2007a. Campagna TRANSMEDOCC-07_SEDIMENTI (TMC-07, I leg), Mediterraneo ccidentale. <http://vector.conismamibi.it/files/diari%20bordo/TMC%20leg1sedim.pdf>.
VECTOR, 2007b. Rapporto finale delle crociere TRANSMEDOCC-07_COLONNA D'ACQUA (TMC-07, II leg) e VECTOR-TM4, Oceano Atlantico – Mediterraneo Occidentale. <http://vector.conismamibi.it/files/diari%20bordo/TMC%20leg2acqua+TM4.pdf>.
VECTOR, 2007c. Rapporto finale di crociera Campagna oceanografica TRANSMEDOCC-07_COLONNA D'ACQUA (TMC-07, III leg), Mediterraneo Orientale. <http://vector.conismamibi.it/files/diari%20bordo/TMC%20leg3acqua.pdf>.
VECTOR, 2007d. Rapporto di crociera Campagna oceanografica TRANSMEDOR-07_SEDIMENTI (TMC-07, IV leg). <http://vector.conismamibi.it/files/diari%20bordo/TMC%20leg4sedim.pdf>.
Velegrakis, A.F., Oikonomou, E., Theocharis, A., Collins, M.B., Kontoyiannis, H., Papadopoulos, V., Voulgaris, G., Wells, T., Balopoulos, E., 1999. Internal waves revealed by Synthetic Aperture Radar (SAR) imagery in the vicinity of the eastern Cretan Arc Straits (Eastern Mediterranean). Progress in Oceanography 44, 553–572.
Vetrano, A., Napoletano, E., Iacono, R., Schroeder, K., Gasparini, G.P., http://dx.doi.org/10.1029/2009JC005680, 2010. Tyrrhenian Sea Circulation and water mass fluxes in spring 2004: observations and model results. Journal of Geophysical Research.